Competition between collective and noncollective excitation modes at high spin in ^{124}Ba

A. Al-Khatib, A. K. Singh,* H. Hübel, P. Bringel, A. Bürger, J. Domscheit, A. Neußer-Neffgen, and G. Schönwaßer
Helmholtz-Institut für Strahlen- und Kernphysik, Universität Bonn, Nussallee 14-16, D-53115 Bonn, Germany

G. B. Hagemann, C. Ronn Hansen, B. Herskind, G. Sletten, and J. N. Wilson†
Niels Bohr Institute, Blegdamsvej 17, DK-2100 Copenhagen Ø, Denmark

J. Timár, A. Algora, Zs. Dombrádi, J. Gál, G. Kalinka, J. Molnár, B. M. Nyakó, D. Sohler, and L. Zolnai
Institute of Nuclear Research of the Hungarian Academy of Sciences, H-4001 Debrecen, Hungary

R. M. Clark, M. Cromaz, P. Fallon, I. Y. Lee, A. O. Macchiavelli, and D. Ward
Nuclear Science Division, Lawrence Berkeley National Laboratory, Berkeley, California 94720, USA

H. Amro‡ and W. C. Ma
Department of Physics, Mississippi State University, Mississippi State, Mississippi 39762, USA

M. Kmiecik, A. Maj, J. Styczen, and K. Zuber
Niewodniczanski Institute of Nuclear Physics, Polish Academy of Sciences, PL-31342 Krakow, Poland

K. Hauschild, A. Korichi, A. Lopez-Martens, J. Roccaz, and S. Siem§
CSNSM Orsay, IN2P3/CNRS, F-91405 Orsay, France

F. Hannachi and J. N. Scheurer
Centre d'Etudes Nucléaires de Bordeaux-Gradignan, F-33175 Gradignan, France

P. Bednarczyk,‖ Th. Byrski, D. Curien, O. Dorvaux, G. Duchêne, B. Gall, F. Khalfallah, I. Piqueras, and J. Robin
Institut de Recherches Subatomiques, CNRS-IN2P3, F-67037 Strasbourg, France

A. Görgen
DAPNIA/SPhN, CEA-Saclay, F-91191 Gif-sur-Yvette, France

K. Juhász
Department of Information Technology, Faculty of Informatics, University of Debrecen, H-4032 Debrecen, Hungary

S. B. Patel
Department of Physics, University of Mumbai, Mumbai, India

A. O. Evans and G. Rainovski
Oliver Lodge Laboratory, University of Liverpool, Liverpool L69 7ZE, United Kingdom

G. Benzoni, A. Bracco, F. Camera, S. Leoni, P. Mason, B. Million, A. Paleni, R. Sacchi, and O. Wieland
Dipartimento di Fisica, Università degli Studi di Milano and INFN, Sezione di Milano, via Celoria 16, I-20133 Milano, Italy

C. M. Petrache and D. Petrache
Dipartimento di Fisica, Università di Camerino and INFN, Sezione di Perugia, I-62032 Camerino, Italy

G. La Rana and R. Moro
Physical Science Department and INFN, Complesso Universitario di Monte S. Angelo, via Cinthia, I-80126 Napoli, Italy

G. De Angelis
Istituto Nazionale di Fisica Nucleare, Laboratori Nazionali de Legnaro, via Romea 4, I-35020 Legnaro, Italy

J. C. Lisle
Schuster Laboratory, University of Manchester, Brunswick Street, Manchester M13 9PL, United Kingdom

B. Cederwall and K. Lagergren
Department of Physics, Royal Institute of Technology, SE-10691 Stockholm, Sweden

R. M. Lieder, E. Podsvirova, W. Gast, and H. Jäger
Institut für Kernphysik, Forschungszentrum Jülich, D-52425 Jülich, Germany

N. Redon
IPN Lyon, IN2P3/CNRS, Universitè de Lyon-1, F-69622 Villeurbanne, France
(Received 10 February 2006; published 11 July 2006)

High-spin states in ^{124}Ba were investigated in two experiments using the ^{64}Ni(^{64}Ni, $4n$)^{124}Ba reaction at three different beam energies. In-beam γ-ray coincidences were measured with the Euroball and Gammasphere detector arrays. In the experiment with Euroball, the CsI detector array Diamant was employed to discriminate against charged-particle channels. Six new rotational bands were observed in ^{124}Ba, and previously known bands were extended to higher spins. One of the bands shows a transition from collective to noncollective behavior at high spins. Configuration assignments are suggested on the basis of comparison with cranked shell model and cranked Nilsson-Strutinsky calculations.

DOI: 10.1103/PhysRevC.74.014305 PACS number(s): 23.20.Lv, 23.20.En, 27.60.+j, 21.60.Ev

I. INTRODUCTION

Transitional nuclei between spherical and strongly deformed regions of the nuclear chart are usually soft with respect to deformation changes. Shape changes, including triaxiality, can be induced by the excitation of nucleons into specific deformation-driving orbitals. In the mass region around $A = 125$, both protons and neutrons can occupy the unique-parity $h_{11/2}$ intruder orbitals which play an important role in driving the nuclear shape. The proton Fermi surface lies in the lower part of the $h_{11/2}$ subshell, which favors prolate shape, whereas the neutron Fermi surface lies in the middle or upper part of the $h_{11/2}$ subshell, which favors oblate shape. Thus, a coexistence of different shapes is expected in these nuclei because of opposite shape-driving forces of protons and neutrons in $h_{11/2}$ orbitals.

Several studies of the development of the shape and collectivity as a function of neutron and proton number have been made in this mass region, e.g., for Xe, Ba, and Ce nuclei [1–18]. It was found that deformation increases with increasing proton number toward $Z = 66$, whereas it decreases with increasing neutron number toward the $N = 82$ shell closure. Total Routhian surface (TRS) calculations show that after the proton $h_{11/2}$ alignment, the nuclei remain prolate ($\gamma \simeq 0^\circ$) whereas the alignment of $h_{11/2}$ neutrons favors a triaxial shape with $\gamma \simeq -30^\circ$ [9,12].

For nuclei with a small number of particles outside the semiclosed core with $Z = 50$ and $N = 64$, the alignment of these particles along the rotation axis at high spin can polarize the nuclei toward an oblate shape. In this spin range, the rotational bands lose collectivity, and single-particle alignments are favored as an efficient way to generate angular momentum. The collective bands terminate when all the single-particle angular momenta involved are aligned along the rotation axis. Higher-spin states can then be generated only by breaking the core.

Transitions from prolate to oblate shape have been observed to take place in two different ways: as smooth band termination, e.g., in the $A \simeq 110$ region [19], and as sudden band termination, e.g., in the $A \simeq 160$ region [20]. In the $A = 125$ region, the low-energy level structure is dominated by collective rotational bands with a moderate prolate deformation ($\varepsilon_2 \simeq 0.25$ and $\gamma \simeq 0^\circ$). However, noncollective excitations have been found to compete with collective rotation at high spin, e.g., in Xe [3] and Cs [21] isotopes, and may become yrast when the proton number increases. One of the aims of the present work was to explore such features in ^{124}Ba. Eight rotational bands were previously known in this nucleus [10]. In this work, they were extended to much higher spins. In addition, six new bands were discovered, and a transition to noncollective excitations was observed in the yrast band. A preliminary report on this work has been given at a recent conference [22].

In the following section, the experimental details and the data analysis are described, followed by a presentation of the experimental results and the level scheme in Sec. III. In Sec. IV, the configurations of the observed structures are discussed, and a brief summary is given in the last section.

II. EXPERIMENTAL DETAILS AND DATA ANALYSIS

Two experiments were performed in which high-spin states in ^{124}Ba were populated using the ^{64}Ni(^{64}Ni, $4n$) reaction at beam energies of 255, 261, and 265 MeV. The higher beam energies were chosen to enhance the population of very-high-spin structures, since the primary goal of both experiments was to search for hyperdeformation. The search for hyperdeformation is still in progress [23]. A number of different reaction channels are open at these beam energies, among them the $4n$ channel leading to ^{124}Ba which is the

*Present address: Department of Physics, IIT Kharagpur, Kharagpur-721302, India.
†Present address: LPSC/IN2P3, F-38026 Grenoble Cedex, France.
‡Present address: Department of Physics, Univ. of Notre Dame, Notre Dame, IN 46556-5670, USA.
§Permanent address: Department of Physics, University of Oslo, N-0316 Oslo, Norway.
‖Permanent address: Niewodniczanski Institute of Nuclear Physics, Polish Academy of Sciences, PL-31342 Krakow, Poland. Present address: GSI, D-64291 Darmstadt, Germany.

strongest of the neutron-evaporation channels. In this work, we focus on the normal-deformed states in this nucleus.

The first experiment was carried out at Lawrence Berkeley National Laboratory. The ^{64}Ni beam of 265 MeV was provided by the 88-Inch. cyclotron. Gamma-ray coincidences were measured using the Gammasphere spectrometer with 100 Compton-suppressed Ge detectors [24]. The target consisted of a ^{64}Ni foil of 476 μg/cm^2 thickness, enriched to 96.5%. Data were recorded with a trigger condition of six or more Ge detectors after Compton suppression and 15 or more "modules" showing a signal. A module is defined as a Ge detector and the bismuth germanate (BGO) scintillators of the suppression shields. After presorting and setting a prompt time window, a total of 1.2×10^9 events with Ge fold $\geqslant$4 were obtained.

The second experiment was performed at the Institut de Recherches Subatomiques at Strasbourg. The ^{64}Ni beams with energies of 255 and 261 MeV were provided by the Vivitron Tandem accelerator. A self-supporting foil of $\simeq$500 μg/cm^2 thickness was used as a target. Gamma-ray coincidences were measured using the Euroball spectrometer [25,26]. It consists of 30 Compton-suppressed conventional (tapered) Ge detectors and 41 composite Ge detectors. Of the latter, the 26 Clover detectors are composed of four Ge crystals each, and the 15 Cluster detectors consist of seven Ge crystals each. At the time of the experiment, 230 individual Ge crystals out of the total of 239 of the full array could be used. An "inner ball" of 210 BGO scintillation detectors was used as a multiplicity filter to enhance the selection of high-spin events. In addition, the charged-particle array Diamant [27,28] consisting of 84 CsI scintillation detectors covering a geometrical solid angle of 95% was placed inside the target chamber. Each crystal has a size of 14.5×14.5 mm^2 and a thickness of 3 mm. The CsI detectors were wrapped in 1.5 μm thick aluminized Mylar foil for light reflection. In front of the forward detectors (up to 67.5°), Ta foils with thicknesses between 5 and 15 μm were mounted to reduce the background of scattered beam particles and δ electrons. Coincidence events were recorded with the requirement that at least three Ge crystals and 11 BGO detectors of the inner ball were in coincidence.

In the off-line analysis, a presorting of the data—which included Compton suppression, pile-up rejection, gain matching, and calibration of the Ge detectors—was made. For the investigation of ^{124}Ba, the information from the Diamant detectors was used to reject events in which charged particles were detected. After setting a wide gate on the prompt time peaks, $\sim 3 \times 10^9$ events of three- and higher-fold Ge-detector concidences remained. The coincidence events from both experiments were unpacked and sorted off line into two-, three- and four-dimensional arrays (matrices, cubes, and hypercubes, respectively) using the RADWARE program package [29].

To obtain information on the multipole order of γ-ray transitions, an asymmetric matrix was sorted with events registered in the detectors at forward (average angle 35°) and backward (average angle 156°) angles on one axis and those detected near 90° on the other axis. Directional correlation (DCO) ratios, defined as $R_{\rm DCO} = I(\gamma_2{}^{\rm fb}, \gamma_1^{90^\circ})/I(\gamma_2{}^{90^\circ}, \gamma_1^{\rm fb})$, where $I(\gamma_2, \gamma_1)$ denotes the intensity of γ_2 in the spectrum gated on γ_1, were determined by setting gates on stretched $E2$ transitions. For a multipolarity determination of low-intensity transitions, two angular correlation matrices were sorted. The first one contained events detected at forward and backward angles on one axis and those registered in all detectors on the other axis. Similarly, the second matrix contained events detected around 90° on one axis and those of all detectors on the other axis. Gates were set in these matrices on the axis with events detected in all detectors. The intensity ratio $R_A = I(\gamma_2{}^{\rm fb}, \gamma_1^{\rm all})/I(\gamma_2{}^{90^\circ}, \gamma_1^{\rm all})$ was used to distinguish between stretched dipole and stretched quadrupole transitions. Values of the DCO and the angular correlation ratios were around 0.6 and 1.0 for stretched dipole and stretched quadrupole transitions, respectively.

III. RESULTS AND LEVEL SCHEME

The energy-level scheme of ^{124}Ba presented in Fig. 1, is based on the results of the present work except for the lower-spin part which was adopted from previous work [10,16,30]. Eight of the 14 rotational bands were known previously. They were partly extended at low and high spins. The level scheme was constructed on the basis of coincidence relationships and relative γ-ray intensities. Spin assignments were based on DCO and angular correlation ratios. For transitions between low-spin states, no angular-correlation information could be obtained because of the loss of the spin alignment from the reaction. While the alignment stays approximately constant at high spins, it is reduced at low spins by the interaction between the nuclear moments and the fields produced by the atomic electrons. Transition energies and their relative intensities, DCO ratios, multipolarities, and placements in the level scheme are listed in Table I. In several cases, in particular for bands 12 and 13, it was not possible to obtain reliable intensities, since the connecting transitions to bands with well-established intensities were too weak. However, in some of these cases, DCO or angular correlation ratios could be determined, because they were derived from intensity ratios.

Band 1 was already established in previous work [10] up to the $I^\pi = 34^+$ state. Above this level, we observe several new transitions resulting in an irregular level pattern. Figure 2 shows two γ-ray coincidence spectra that demonstrate the forking of band 1 above the 1444.3 keV transition and into the 1583.4–1610.9 keV sequence. The DCO ratio of the 1444.3 keV transition is compatible with a stretched quadrupole, presumably $E2$, transition. The multipolarity of the other new transitions could not be determined. Hence, the spin assignments to the high-spin levels are tentative and, therefore, given in parentheses in Fig. 1.

Band 2, which was known up to the $I^\pi = 24^+$ state [10], is extended by six transitions to higher spins. For the new transitions, stretched quadrupole, probably $E2$, multipolarity was established up to 1261.2 keV. However, because of the regularity of the band, $E2$ multipolarity may also be assumed for the other high-spin transitions. Several new interband transitions connecting band 2 with band 1 have also been observed.

Bands 3 to 8 were also known from previous work [10,16]. We confirm these sequences and place three to four transitions

TABLE I. Energies, relative intensities, DCO ratios, multipolarities, and spin assignments of γ-ray transitons of ^{124}Ba.

Excitation E_i (keV)	Energy[a] E_γ (keV)	Intensity[b] I_γ	R^{c}_{DCO} ratio	Band$_i$ $\rightarrow$ Band$_f$	Assignment $I_i^\pi \rightarrow I_f^\pi$	Multipolarity
230	229.7	536(31)	–	gsb $\rightarrow$ gsb	$2^+ \rightarrow 0^+$	$E2$
652	421.1	524(28)	–	gsb $\rightarrow$ gsb	$4^+ \rightarrow 2^+$	$E2$
873	643.4	–	–	8 $\rightarrow$ gsb	$2^+ \rightarrow 2^+$	$M1$
873	873.3	–	–	8 $\rightarrow$ gsb	$2^+ \rightarrow 0^+$	$E2$
1162	510.0	–	–	7 $\rightarrow$ gsb	$3^+ \rightarrow 4^+$	$M1$
1162	932.8	–	–	7 $\rightarrow$ gsb	$3^+ \rightarrow 2^+$	$M1$
1228	576.5	500	0.90	gsb $\rightarrow$ gsb	$6^+ \rightarrow 4^+$	$E2$
1325	451.7	–	–	8 $\rightarrow$ 8	$4^+ \rightarrow 2^+$	$E2$
1325	673.1	–	–	8 $\rightarrow$ gsb	$4^+ \rightarrow 4^+$	$M1$
1325	1094.5	–	–	8 $\rightarrow$ gsb	$4^+ \rightarrow 2^+$	$E2$
1672	444.4	–	–	7 $\rightarrow$ gsb	$5^+ \rightarrow 6^+$	$M1$
1672	510.0	–	–	7 $\rightarrow$ 7	$5^+ \rightarrow 3^+$	$E2$
1672	1020.8	–	–	7 $\rightarrow$ gsb	$5^+ \rightarrow 4^+$	$M1$
1722	1491.6	–	–	4a $\rightarrow$ gsb	$(3^-) \rightarrow 2^+$	$E1$
1858	533.4	–	–	8 $\rightarrow$ 8	$6^+ \rightarrow 4^+$	$E2$
1858	629.7	–	–	8 $\rightarrow$ gsb	$6^+ \rightarrow 6^+$	$M1$
1913	684.9	–	–	3 $\rightarrow$ gsb	$5^- \rightarrow 6^+$	$E1$
1913	1260.8	23(5)	0.74	3 $\rightarrow$ gsb	$5^- \rightarrow 4^+$	$E1$
1923	694.7	348(22)	1.00	gsb $\rightarrow$ gsb	$8^+ \rightarrow 6^+$	$E2$
2034	312.0	–	0.45	4 $\rightarrow$ 4a	$4^- \rightarrow (3^-)$	$M1$
2034	1381.9	–	1.11	4 $\rightarrow$ gsb	$4^- \rightarrow 4^+$	$E1$
2262	338.4	2(1)	–	3 $\rightarrow$ gsb	$7^- \rightarrow 8^+$	$E1$
2262	348.4	6(1)	–	3 $\rightarrow$ 3	$7^- \rightarrow 5^-$	$E2$
2262	1033.7	67(16)	0.66	3 $\rightarrow$ gsb	$7^- \rightarrow 6^+$	$E1$
2267	354.0	–	–	5a $\rightarrow$ 3	$5^- \rightarrow 5^-$	$M1$
2267	942.4	–	–	5a $\rightarrow$ 8	$5^- \rightarrow 4^+$	$E1$
2267	1038.6	–	–	5a $\rightarrow$ gsb	$5^- \rightarrow 6^+$	$E1$
2267	1615.3	6(2)	–	5a $\rightarrow$ gsb	$5^- \rightarrow 4^+$	$E1$
2285	612.7	–	–	7 $\rightarrow$ 7	$7^+ \rightarrow 5^+$	$E2$
2285	1057.0	–	–	7 $\rightarrow$ gsb	$7^+ \rightarrow 6^+$	$M1$
2359	325.5	13(2)	1.32	4 $\rightarrow$ 4	$6^- \rightarrow 4^-$	$E2$
2359	446.3	22(4)	0.35	4 $\rightarrow$ 3	$6^- \rightarrow 5^-$	$M1$
2359	1130.0	31(7)	0.99	4 $\rightarrow$ gsb	$6^- \rightarrow 6^+$	$E1$
2479	555.7	–	–	8 $\rightarrow$ gsb	$8^+ \rightarrow 8^+$	$M1$
2479	620.9	–	–	8 $\rightarrow$ 8	$8^+ \rightarrow 6^+$	$E2$
2498	230.5	64(12)	0.58	6 $\rightarrow$ 5a	$6^- \rightarrow 5^-$	$M1$
2498	824.9	–	–	6 $\rightarrow$ 7	$6^- \rightarrow 5^+$	$E1$
2647	288.0	2(1)	–	5a $\rightarrow$ 4	$7^- \rightarrow 6^-$	$M1$
2647	380.4	5(2)	1.05	5a $\rightarrow$ 5a	$7^- \rightarrow 5^-$	$E2$
2647	385.7	7(2)	0.67	5a $\rightarrow$ 3	$7^- \rightarrow 7^-$	$M1$
2647	789.3	8(3)	–	5a $\rightarrow$ 8	$7^- \rightarrow 6^+$	$E1$
2688	764.4	213(32)	0.97	gsb $\rightarrow$ gsb	$10^+ \rightarrow 8^+$	$E2$
2691	193.0	39(14)	0.41	5 $\rightarrow$ 6	$7^- \rightarrow 6^-$	$M1$
2705	345.2	46(8)	0.99	4 $\rightarrow$ 4	$8^- \rightarrow 6^-$	$E2$
2705	442.7	6(3)	0.48	4 $\rightarrow$ 3	$8^- \rightarrow 7^-$	$M1$
2705	781.0	29(6)	0.75	4 $\rightarrow$ gsb	$8^- \rightarrow 8^+$	$E1$
2722	459.8	43(9)	1.13	3 $\rightarrow$ 3	$9^- \rightarrow 7^-$	$E2$
2722	798.0	75(8)	0.50	3 $\rightarrow$ gsb	$9^- \rightarrow 8^+$	$E1$
2906	215.9	23(11)	0.35	6 $\rightarrow$ 5	$8^- \rightarrow 7^-$	$M1$
2906	408.7	6(4)	–	6 $\rightarrow$ 6	$8^- \rightarrow 6^-$	$E2$
2975	689.8	–	–	7 $\rightarrow$ 7	$9^+ \rightarrow 7^+$	$E2$
2975	1053.0	–	–	7 $\rightarrow$ gsb	$9^+ \rightarrow 8^+$	$M1$
3110	203.2	–	–	5 $\rightarrow$ 6	$9^- \rightarrow 8^-$	$M1$
3110	404.9	6(2)	0.77	5 $\rightarrow$ 4	$9^- \rightarrow 8^-$	$M1$
3110	419.2	15(3)	–	5 $\rightarrow$ 5	$9^- \rightarrow 7^-$	$E2$

TABLE I. (*Continued*.)

Excitation E_i (keV)	Energy[a] E_γ (keV)	Intensity[b] I_γ	R^c_{DCO} ratio	Band$_i$ → Band$_f$	Assignment $I_i^\pi \rightarrow I_f^\pi$	Multipolarity
3157	434.7	3(1)	–	4 → 3	$10^- \rightarrow 9^-$	$M1$
3157	452.0	61(17)	1.02	4 → 4	$10^- \rightarrow 8^-$	$E2$
3178	698.7	–	–	8 → 8	$10^+ \rightarrow 8^+$	$E2$
3287	564.9	101(22)	1.09	3 → 3	$11^- \rightarrow 9^-$	$E2$
3287	599.8	–	–	3 → gsb	$11^- \rightarrow 10^+$	$E1$
3335	225.8	13(3)	–	6 → 5	$10^- \rightarrow 9^-$	$M1$
3335	429.4	28(6)	1.01	6 → 6	$10^- \rightarrow 8^-$	$E2$
3437	748.3	196(13)	0.97	1 → gsb	$12^+ \rightarrow 10^+$	$E2$
3591	256.0	13(5)	–	5 → 6	$11^- \rightarrow 10^-$	$M1$
3591	482.2	39(8)	0.95	5 → 5	$11^- \rightarrow 9^-$	$E2$
3692	255.6	6(3)	0.74	2 → 1	$12^+ \rightarrow 12^+$	$M1$
3692	1004.0	16(5)	1.17	2 → gsb	$12^+ \rightarrow 10^+$	$E2$
3694	718.8	–	–	7 → 7	$11^+ \rightarrow 9^+$	$E2$
3772	486.1	–	–	4 → 3	$12^- \rightarrow 11^-$	$M1$
3772	615.5	56(16)	1.03	4 → 4	$12^- \rightarrow 10^-$	$E2$
3891	299.9	16(4)	–	6 → 5	$12^- \rightarrow 11^-$	$M1$
3891	556.4	13(5)	0.97	6 → 6	$12^- \rightarrow 10^-$	$E2$
3968	681.0	94(25)	1.15	3 → 3	$13^- \rightarrow 11^-$	$E2$
4127	434.2	–	–	1 → 2	$14^+ \rightarrow 12^+$	$E2$
4127	689.4	173(13)	1.03	1 → 1	$14^+ \rightarrow 12^+$	$E2$
4228	336.6	7(2)	–	5 → 6	$13^- \rightarrow 12^-$	$M1$
4228	636.3	20(4)	1.15	5 → 5	$13^- \rightarrow 11^-$	$E2$
4382	689.9	–	–	12 → 2	$(11^+) \rightarrow 12^+$	$M1$
4382	945.4	–	–	12 → 1	$(11^+) \rightarrow 12^+$	$M1$
4382	1407.0	–	–	12 → 7	$(11^+) \rightarrow 9^+$	$E2$
4408	281.3	3(1)	0.53	2 → 1	$14^+ \rightarrow 14^+$	$M1$
4408	715.5	14(4)	1.22	2 → 2	$14^+ \rightarrow 12^+$	$E2$
4408	971.1	24(6)	1.38	2 → 1	$14^+ \rightarrow 12^+$	$E2$
4534	566.2	–	–	4 → 3	$14^- \rightarrow 13^-$	$M1$
4534	762.1	48(16)	1.03	4 → 4	$14^- \rightarrow 12^-$	$E2$
4552	170.0	–	–	13 → 12	$(12^+) \rightarrow (11^+)$	$M1$
4552	722.0	–	0.74	13 → 13a	$(12^+) \rightarrow (11)$	–
4552	858.2	–	–	13 → 7	$(12^+) \rightarrow 11^+$	$M1$
4604	375.6	5(2)	–	6 → 5	$14^- \rightarrow 13^-$	$M1$
4604	711.2	13(6)	1.00	6 → 6	$14^- \rightarrow 12^-$	$E2$
4762	793.8	61(9)	1.03	3 → 3	$15^- \rightarrow 13^-$	$E2$
4767	215.0	–	–	12 → 13	$(13^+) \rightarrow (12^+)$	$M1$
4767	384.2	–	1.14	12 → 12	$(13^+) \rightarrow (11^+)$	$E2$
4767	1073.2	–	–	12 → 7	$(13^+) \rightarrow 11^+$	$E2$
4893	766.1	156(13)	1.05	1 → 1	$16^+ \rightarrow 14^+$	$E2$
5010	405.6	3(1)	–	5 → 6	$15^- \rightarrow 14^-$	$M1$
5010	780.9	20(3)	0.92	5 → 5	$15^- \rightarrow 13^-$	$E2$
5028	261.0	–	–	13 → 12	$(14^+) \rightarrow (13^+)$	$M1$
5028	476.0	–	1.05	13 → 13	$(14^+) \rightarrow (12^+)$	$E2$
5216	323.2	3(2)	0.78	2 → 1	$16^+ \rightarrow 16^+$	$M1$
5216	808.5	42(8)	1.35	2 → 2	$16^+ \rightarrow 14^+$	$E2$
5216	1090.0	11(5)	–	2 → 1	$16^+ \rightarrow 14^+$	$E2$
5330	302.0	–	–	12 → 13	$(15^+) \rightarrow (14^+)$	$M1$
5330	562.5	–	1.03	12 → 12	$(15^+) \rightarrow (13^+)$	$E2$
5330	1203.7	–	–	12 → 1	$(15^+) \rightarrow 14^+$	$M1$
5392	630.7	–	–	4 → 3	$16^- \rightarrow 15^-$	$M1$
5392	858.3	31(11)	0.94	4 → 4	$16^- \rightarrow 14^-$	$E2$
5446	436.3	2(1)	–	6 → 5	$16^- \rightarrow 15^-$	$M1$
5446	842.6	9(2)	0.85	6 → 6	$16^- \rightarrow 14^-$	$E2$
5639	878.0	51(12)	1.00	3 → 3	$17^- \rightarrow 15^-$	$E2$

TABLE I. (*Continued*.)

Excitation E_i (keV)	Energy[a] E_γ (keV)	Intensity[b] I_γ	R^c_{DCO} ratio	Band$_i$ → Band$_f$	Assignment $I_i^\pi \rightarrow I_f^\pi$	Multipolarity
5669	339.0	–	–	13 → 12	$(16^+) \rightarrow (15^+)$	$M1$
5669	640.9	–	1.00	13 → 13	$(16^+) \rightarrow (14^+)$	$E2$
5726	832.0	48(9)	0.27	9 → 1	$17^+ \rightarrow 16^+$	$M1$
5764	871.6	84(15)	1.10	1 → 1	$18^+ \rightarrow 16^+$	$E2$
5906	459.8	–	–	5 → 6	$17^- \rightarrow 16^-$	$M1$
5906	895.7	18(3)	1.12	5 → 5	$17^- \rightarrow 15^-$	$E2$
6046	377.0	–	–	12 → 13	$(17^+) \rightarrow (16^+)$	$M1$
6046	715.5	–	1.01	12 → 12	$(17^+) \rightarrow (15^+)$	$E2$
6081	317.2	–	–	2 → 1	$18^+ \rightarrow 18^+$	$M1$
6081	864.7	37(9)	0.93	2 → 2	$18^+ \rightarrow 16^+$	$E2$
6081	1187.9	–	–	2 → 1	$18^+ \rightarrow 16^+$	$E2$
6192	1299.0	–	–	10 → 1	$18^+ \rightarrow 16^+$	$E2$
6290	896.6	20(8)	1.21	4 → 4	$18^- \rightarrow 16^-$	$E2$
6383	477.2	–	–	6 → 5	$18^- \rightarrow 17^-$	$M1$
6383	938.1	9(2)	–	6 → 6	$18^- \rightarrow 16^-$	$E2$
6454	408.0	–	–	13 → 12	$(18^+) \rightarrow (17^+)$	$M1$
6454	784.9	–	1.04	13 → 13	$(18^+) \rightarrow (16^+)$	$E2$
6556	917.3	29(6)	1.15	3 → 3	$19^- \rightarrow 17^-$	$E2$
6583	819.1	7(2)	–	9 → 1	$19^+ \rightarrow 18^+$	$M1$
6583	857.7	22(9)	0.95	9 → 9	$19^+ \rightarrow 17^+$	$E2$
6705	1066.0	–	–	$3a$ → 3	$(18) \rightarrow 17^-$	–
6712	948.6	59(13)	1.06	1 → 1	$20^+ \rightarrow 18^+$	$E2$
6871	487.8	–	–	5 → 6	$19^- \rightarrow 18^-$	$M1$
6871	965.0	7(2)	0.96	5 → 5	$19^- \rightarrow 17^-$	$E2$
6898	444.0	–	–	12 → 13	$(19^+) \rightarrow (18^+)$	$M1$
6898	852.0	–	1.06	12 → 12	$(19^+) \rightarrow (17^+)$	$E2$
7000	919.4	25(6)	1.08	2 → 2	$20^+ \rightarrow 18^+$	$E2$
7000	1236.2	–	–	2 → 1	$20^+ \rightarrow 18^+$	$E2$
7084	891.9	20(10)	0.91	10 → 10	$20^+ \rightarrow 18^+$	$E2$
7084	1319.7	–	0.92	10 → 1	$20^+ \rightarrow 18^+$	$E2$
7230	940.5	13(6)	0.90	4 → 4	$20^- \rightarrow 18^-$	$E2$
7365	910.0	–	1.08	13 → 13	$(20^+) \rightarrow (18^+)$	$E2$
7366	495.2	–	–	6 → 5	$20^- \rightarrow 19^-$	$M1$
7366	982.6	4(2)	–	6 → 6	$20^- \rightarrow 18^-$	$E2$
7502	945.3	16(4)	1.26	3 → 3	$21^- \rightarrow 19^-$	$E2$
7503	791.3	–	–	9 → 1	$21^+ \rightarrow 20^+$	$M1$
7503	918.0	12(4)	0.87	9 → 9	$21^+ \rightarrow 19^+$	$E2$
7717	1004.9	41(10)	1.08	1 → 1	$22^+ \rightarrow 20^+$	$E2$
7865	966.9	–	1.16	12 → 12	$(21^+) \rightarrow (19^+)$	$E2$
7878	1007.4	–	–	5 → 5	$21^- \rightarrow 19^-$	$E2$
7984	983.7	18(4)	1.09	2 → 2	$22^+ \rightarrow 20^+$	$E2$
7984	1272.3	–	–	2 → 1	$22^+ \rightarrow 20^+$	$E2$
8101	1016.8	11(5)	1.08	10 → 10	$22^+ \rightarrow 20^+$	$E2$
8101	1389.0	–	–	10 → 1	$22^+ \rightarrow 20^+$	$E2$
8263	1034.4	11(5)	0.91	4 → 4	$22^- \rightarrow 20^-$	$E2$
8371	1006.3	–	1.06	13 → 13	$(22^+) \rightarrow (20^+)$	$E2$
8411	1044.0	–	–	6 → 6	$22^- \rightarrow 20^-$	$E2$
8486	769.2	–	–	9 → 1	$23^+ \rightarrow 22^+$	$M1$
8486	983.4	10(4)	1.11	9 → 9	$23^+ \rightarrow 21^+$	$E2$
8512	1009.7	14(4)	0.95	3 → 3	$23^- \rightarrow 21^-$	$E2$
8795	1077.1	37(9)	1.22	1 → 1	$24^+ \rightarrow 22^+$	$E2$
8905	1040.6	–	1.22	12 → 12	$(23^+) \rightarrow (21^+)$	$E2$
8913	1034.0	–	–	5 → 5	$23^- \rightarrow 21^-)$	$E2$
9054	1069.2	12(3)	0.90	2 → 2	$24^+ \rightarrow 22^+$	$E2$
9179	1078.6	10(5)	0.84	10 → 10	$24^+ \rightarrow 22^+$	$E2$
9179	1462.3	–	–	10 → 1	$24^+ \rightarrow 22^+$	$E2$

TABLE I. (*Continued*.)

Excitation E_i (keV)	Energy[a] E_γ (keV)	Intensity[b] I_γ	R^c_{DCO} ratio	Band$_i$ → Band$_f$	Assignment $I_i^\pi \rightarrow I_f^\pi$	Multipolarity
9381	1117.6	5(1)	0.89	4 → 4	$24^- \rightarrow 22^-$	$E2$
9430	1058.5	–	1.25	13 → 13	$(24^+) \rightarrow (22^+)$	$E2$
9528	1117.1	–	–	6 → 6	$(24^-) \rightarrow (22^-)$	$E2$
9566	1078.2	6(2)	1.25	9 → 9	$25^+ \rightarrow 23^+$	$E2$
9613	1100.1	8(2)	1.37	3 → 3	$25^- \rightarrow 23^-$	$E2$
9918	1124.1	–	–	11 → 1	$(25) \rightarrow 24^+$	–
9951	1154.5	15(6)	1.11	1 → 1	$26^+ \rightarrow 24^+$	$E2$
9976	1070.6	–	1.07	12 → 12	$(25^+) \rightarrow (23^+)$	$E2$
9984	1070.7	–	–	5 → 5	$(25^-) \rightarrow (23^-)$	$E2$
10223	1168.6	10(3)	0.97	2 → 2	$26^+ \rightarrow 24^+$	$E2$
10312	1131.4	5(2)	1.16	10 → 10	$26^+ \rightarrow 24^+$	$E2$
10312	1516.9	–	–	10 → 1	$26^+ \rightarrow 24^+$	$E2$
10521	1091.9	–	1.12	13 → 13	$(26^+) \rightarrow (24^+)$	$E2$
10563	1181.2	4(1)	–	4 → 4	$26^- \rightarrow 24^-$	$E2$
10707	1178.4	–	–	6 → 6	$(26^-) \rightarrow (24^-)$	$E2$
10751	1184.8	2(2)	–	9 → 9	$27^+ \rightarrow 25^+$	$E2$
10814	1201.5	6(2)	1.29	3 → 3	$27^- \rightarrow 25^-$	$E2$
11029	1151.3	–	–	11 → 11	$(27) \rightarrow (25)$	$E2$
11079	1102.4	–	1.13	12 → 12	$(27^+) \rightarrow (25^+)$	$E2$
11118	1505.0	–	–	3b → 3	$(26) \rightarrow 25^-$	–
11183	1231.2	11(4)	0.86	1 → 1	$28^+ \rightarrow 26^+$	$E2$
11475	1251.8	6.3(3.8)	0.97	2 → 2	$28^+ \rightarrow 26^+$	$E2$
11526	1214.2	3(2)	0.91	10 → 10	$28^+ \rightarrow 26^+$	$E2$
11651	1129.3	–	1.21	13 → 13	$(28^+) \rightarrow (26^+)$	$E2$
11755	1192.0	2(1)	–	4 → 4	$28^- \rightarrow 26^-$	$E2$
12035	1282.9	–	–	9 → 9	$29^+ \rightarrow 27^+$	$E2$
12118	1304.4	5(1)	1.02	3 → 3	$29^- \rightarrow 27^-$	$E2$
12246	1164.9	–	–	12 → 12	$(29^+) \rightarrow (27^+)$	$E2$
12290	1221.2	–	–	11 → 11	$(29) \rightarrow (27)$	$E2$
12492	1309.6	10(3)	1.27	1 → 1	$30^+ \rightarrow 28^+$	$E2$
12738	1261.2	4(1)	0.93	2 → 2	$30^+ \rightarrow 28^+$	$E2$
12826	1297.9	–	–	10 → 10	$30^+ \rightarrow 28^+$	$E2$
12862	1210.9	–	–	13 → 13	$(30^+) \rightarrow (28^+)$	$E2$
12961	1206.5	–	–	4 → 4	$(30^-) \rightarrow (28^-)$	$E2$
13350	1232.0	–	0.8[d]	14 → 3	$(30) \rightarrow 29^-$	–
13413	1377.0	–	–	9 → 9	$31^+ \rightarrow 29^+$	$E2$
13498	1249.5	–	–	12 → 12	$(31^+) \rightarrow (29^+)$	$E2$
13519	1400.8	4(2)	1.18	3 → 3	$31^- \rightarrow 29^-$	$E2$
13592	1301.4	–	–	11 → 11	$(31) \rightarrow (29)$	$E2$
13881	1388.6	9(3)	1.22	1 → 1	$32^+ \rightarrow 30^+$	$E2$
14063	1324.5	3.6(2.9)	–	2 → 2	$32^+ \rightarrow 30^+$	$E2$
14185	1224.3	–	–	4 → 4	$32^- \rightarrow 30^-$	$E2$
14196	1370.1	–	–	10 → 10	$32^+ \rightarrow 30^+$	$E2$
14757	1238.0	–	0.94[d]	14 → 3	$(32) \rightarrow 31^-$	–
14757	1406.9	–	–	14 → 14	$(32) \rightarrow (30)$	$E2$
14838	1340.6	–	–	12 → 12	$(33^+) \rightarrow (31^+)$	$E2$
14887	1474.7	–	–	9 → 9	$33^+ \rightarrow 31^+$	$E2$
14981	1389.1	–	–	11 → 11	$(33) \rightarrow (31)$	$E2$
15007	1486.5	–	–	3 → 3	$33^- \rightarrow 31^-$	$E2$
15336	1454.8	6(2)	1.38[e]	1 → 1	$34^+ \rightarrow 32^+$	$E2$
15465	1401.6	–	–	2 → 2	$34^+ \rightarrow 32^+$	$E2$
15476	1290.9	–	–	4 → 4	$(34^-) \rightarrow 32^-$	$E2$
15624	1427.5	–	–	10 → 10	$34^+ \rightarrow 32^+$	$E2$
16031	1274.0	–	1.42[d]	14 → 14	$(34) \rightarrow (32)$	$E2$
16286	1448.0	–	–	12 → 12	$(35^+) \rightarrow (33^+)$	$E2$
16434	1544.2	–	–	9 → 9	$(35^+) \rightarrow 33^+$	$E2$

TABLE I. (*Continued.*)

Excitation E_i (keV)	Energy[a] E_γ (keV)	Intensity[b] I_γ	R^c_{DCO} ratio	Band$_i$ → Band$_f$	Assignment $I_i^\pi \rightarrow I_f^\pi$	Multipolarity
16463	1481.8	–	–	11 → 11	(35) → (33)	$E2$
16780	1444.3	5(2)	1.41[e]	1 → 1	$36^+ \rightarrow 34^+$	$E2$
16918	1583.4	–	–	1c → 1	$(36^+) \rightarrow 34^+$	$E2$
16949	1484.3	–	–	2 → 2	$36^+ \rightarrow 34^+$	$E2$
17117	1493.3	–	–	10 → 10	$(36^+) \rightarrow 34^+$	$E2$
17437	1406.0	–	–	14 → 14	(36) → (34)	$E2$
18042	1579.7	–	–	11 → 11	(37) → (35)	$E2$
18055	1619.6	–	–	9 → 9	$(37^+) \rightarrow (35^+)$	$E2$
18075	1294.4	–	–	1a → 1	$(38^+) \rightarrow 36^+$	$E2$
18149	1368.4	–	–	1b → 1	$(38^+) \rightarrow 36^+$	$E2$
18529	1610.9	–	–	1c → 1c	$(38^+) \rightarrow (36^+)$	$E2$
18656	1537.7	–	–	10 → 10	$(38^+) \rightarrow (36^+)$	$E2$
18911	1474.0	–	–	14 → 14	(38) → (36)	$E2$
19722	1679.7	–	–	11 → 11	(39) → (37)	$E2$
20485	1574.0	–	–	14 → 14	(40) → (38)	$E2$
21503	1780.9	–	–	11 → 11	(41) → (39)	$E2$
22152	1666.8	–	–	14 → 14	(42) → (40)	$E2$
23386	1883.2	–	–	11 → 11	(43) → (41)	$E2$
25372	1986.3	–	–	11 → 11	(45) → (43)	$E2$

[a]Uncertainties of γ-ray energies are between 0.1 and 0.6 keV depending on their intensity.
[b]Intensities are normalized to the 576.5 keV transition with $I_\gamma = 500$.
[c]Uncertainties in the DCO ratios are between 0.03 and 0.2.
[d]Uncertainty >50% due to low statistics.
[e]Ratio obtained from angular distribution matrices.

on top of the previously known levels of bands 3, 5, and 6. The low-spin part of the coupled bands 5 and 6 was rearranged. Two close-lying 7^- states, at 2647 and 2691 keV, were previously known [10]. The 2647 keV level was assigned as a member of the $\alpha = 1$ signature branch, whereas it was suggested that the 2691 keV state does not belong to the band. Analyzing triple coincidences, we found a 419.2 keV transition from the 9^- band member to the 7^- level at 2691 keV which was previously not detected, probably because it lies so close in energy to the strong 421.1 keV $4^+ \rightarrow 2^+$ transition. We rearranged the 7^- states as shown in the level scheme of Fig. 1. In this way, the coupled bands continue with $\Delta I = 1$ and $\Delta I = 2$ transitions down to the 5^- state. The fairly strong transition of 462.0 keV to the 7^- state at 2647 keV may be explained by mixing of the 7^- levels.

Band 4 is extended by seven transitions. Bands 7 and 8 are weakly populated and could not be extended to higher spin. DCO ratios measured for some of the inband transitions as well as decay-out transitions are in accordance with the previous spin assignments [10]. For some high-spin transitions observed in this work, we could not determine the multipolarity. However, $E2$ multipolaritiy has been assumed for the inband transitions because of the regularity of the bands.

The two sequences of γ rays labeled bands 9 and 10 have been observed for the first time in our work. Both bands decay into levels of band 1. Gamma-ray coincidence spectra for the two bands are shown in Fig. 3. The 832.0 keV transition, which we place at the bottom of band 9, was observed already by Pilotte *et al.* [10]. The linear polarization asymmetry of this transition, measured with the Euroball Clover detectors, is small and negative, which confirms the previously suggested mixed $M1/E2$ multipolarity for this transition which feeds into the 16^+ state of band 1. For an electric dipole, one would expect no mixing and, thus, a positive asymmetry [31]. This leads to $I^\pi = 17^+$ for the lowest level of band 9. Band 10 decays into band 1 via several transitions between 1299.0 and 1516.9 keV. Of these, only the 1319.7 keV transition is clean and strong enough to allow the determination of the angular correlation ratio. This ratio is compatible with stretched quadrupole, probably $E2$, multipolarity. Thus, we assign even spins and positive parity to band 10. Only the inband transitions near the bottom of bands 9 and 10 are sufficiently strong for a determination of the angular correlation ratios. They are consistent with stretched quadrupole, probably $E2$, transitions.

The three new bands—11, 12, and 13—are only tentatively connected to lower-lying levels, and their excitation energies, spins, and parities remain uncertain. Gamma-ray coincidence spectra of these bands are displayed in Figs. 4 and 5. Band 11 is a cascade of 11 transitions, probably of $E2$ multipolarity, which decays into band 1. Transitions of band 1 are observed in coincidence with the new band up to the 24^+ level. The transitions of band 11 show an energy difference that is smoothly increasing from 71 to 105 keV; only the difference between the 1124.1 and 1151.3 keV transitions is much lower. Therefore, the 1124.1 kev γ ray may be a link between the two bands. Other weak γ-ray lines observed in the coincidence spectra (see Fig. 4) with energies of 1095, 1453, 1516, 1833 and 1914 keV might also be candidates for interband transitions.

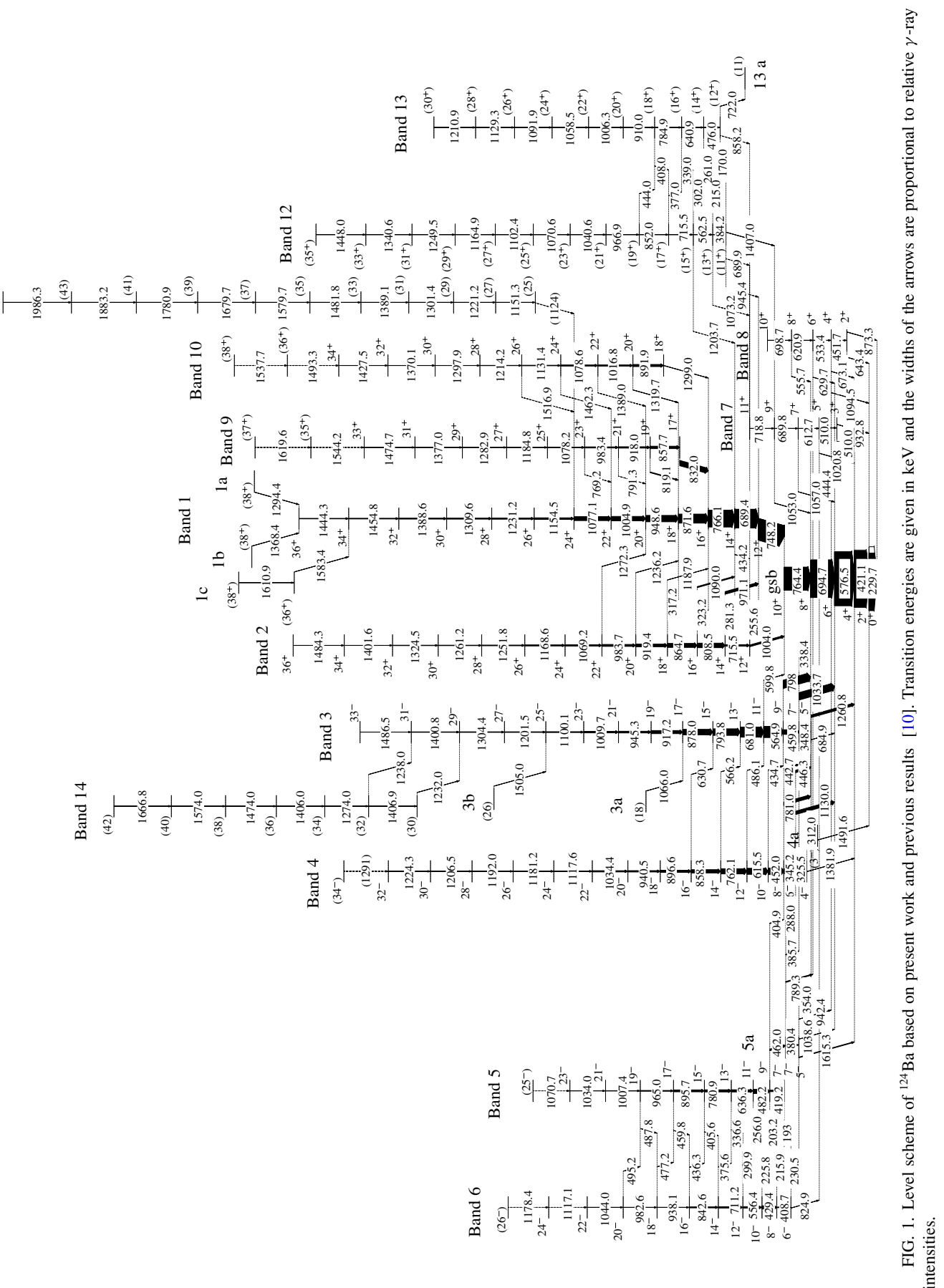

FIG. 1. Level scheme of ^{124}Ba based on present work and previous results [10]. Transition energies are given in keV and the widths of the arrows are proportional to relative γ-ray intensities.

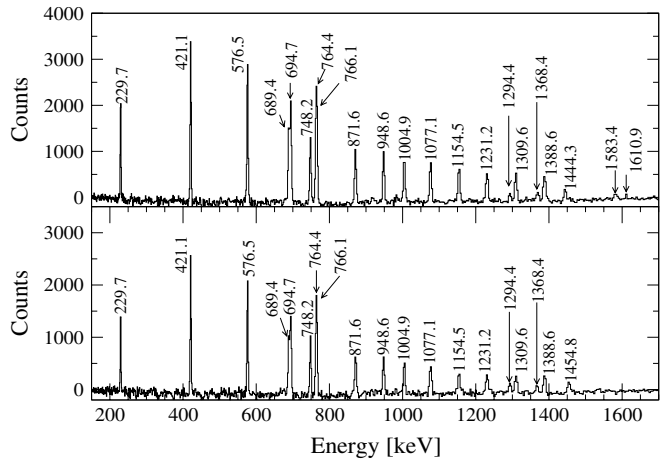

FIG. 2. Summed triple-gated γ-ray coincidence spectra of band 1. Upper spectrum was produced by setting two gates on transitions (689.4 to 1444.3 keV) of band 1 and one gate on the 1454.8 keV transition; Lower spectrum, by setting two gates on transitions (689.4 to 1454.8 keV) of band 1 and one gate on the 1444.3 keV transition.

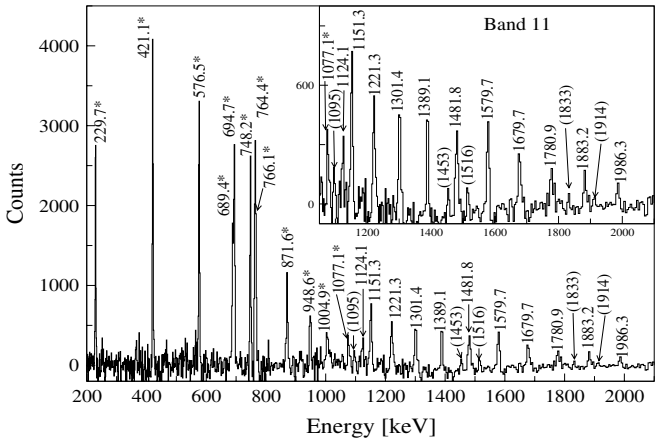

FIG. 4. Summed triple-gated coincidence spectrum of band 11, produced by setting one gate on transitions (229.7 to 1077.1 keV) of band 1 and two gates on transitions (1124.1 to 1986.3 keV) of band 11. Asterisks mark peaks of band 1. Energies in parentheses correspond to transitions observed in coincidence but not placed in the level scheme.

Bands 12 and 13 are connected by weak interband transitions in the low-spin region and, thus, probably form a pair of signature-partner bands. They decay into bands 1, 2, and 7. Of the linking transitions shown in the level scheme (Fig. 1), only the 1407.0 keV line is firmly established. Because of the low intensity, its DCO ratio has a large uncertainty and the multipolarity could not be unambiguously determined. Hence, the spin assignment to the bands is tentative. The other linking transitions are weak and only tentatively assigned. Transitions of band 1 up to the 10^+ and possibly up to the 14^+ state are observed in coincidence with bands 12 and 13 (Fig. 5).

Band 14 has been observed for the first time in this work. It decays into band 3. Because of the low intensities of the linking transitions, the DCO ratios have large uncertainties and their multipolarities could not be reliably determined. Since band 14 feeds into the $I^\pi = 29^-$ state of band 3, we tentatively assign $I = 30$ to the lowest level of the band.

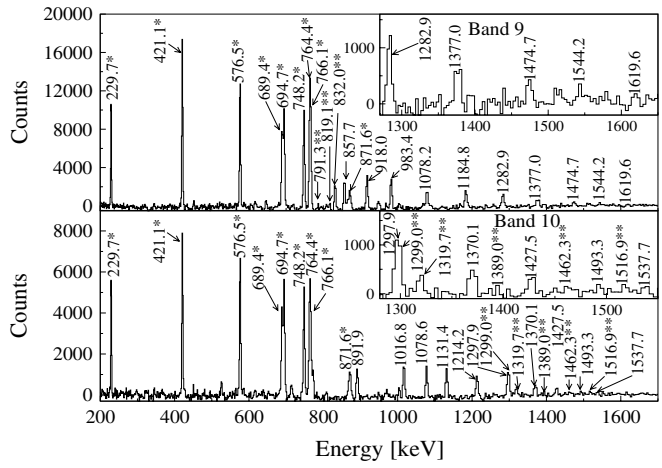

FIG. 3. Sum of triple-gated γ-ray coincidence spectra of band 9 (upper panel) and band 10 (lower panel). Band 9 spectrum was produced by setting one gate on transitions (229.7 to 766.1 keV) of band 1 and two gates on transitions (832.0 to 1619.6 keV) of band 9. Band 10 spectrum was obtained with one gate on the same transitions of band 1 and two gates on transitions (891.9 to 1537.7 keV) of band 10. Single asterisks mark peaks of band 1. γ rays marked by double asterisks are the linking transitions from bands 9 and 10 to band 1.

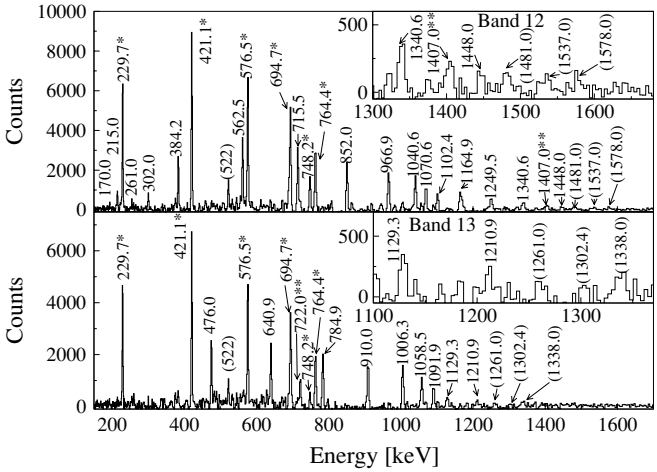

FIG. 5. Summed double- and triple-gated coincidence spectra of bands 12 and 13. Band 12 spectrum (upper panel) was produced by setting one gate on transitions (229.7 to 764.4 keV) of band 1 and two gates on transitions (384.2 to 1448.0 keV) of band 12. Band 13 spectrum (lower panel) was obtained by setting one gate on the same transitions of band 1 and two gates on transitions (476.0 to 1210.9 keV) of band 13. Single asterisks mark peaks of band 1. Double asterisks mark the decay-out transitions. Energies in parentheses correspond to transitions observed in coincidence but not placed in the level scheme.

IV. DISCUSSION

In previous work [10,16,30,32], configuration assignments were made to the low- and medium-spin regions of bands 1 to 8 of ^{124}Ba. Arguments for the configuration assignments are the observed excitation energies, spins, parities, band-crossing frequencies, and alignment gains. These quantities can be compared to those observed in neighboring nuclei as well as to cranked shell model (CSM) [33,34] and cranked Nilsson-Strutinsky (CNS) [19,35] calculations. For the coupled bands, signature splittings and $B(M1)/B(E2)$ ratios provide additional evidence for their configurations.

In the discussion of the configurations of the observed bands, we distinguish between the low- and high-spin regions. At low and medium spins, pairing correlations are important and comparison of experiment with theory is usually made within the framework of the CSM. Here, we adopt the results of previous work [10] for bands 1 to 8 and make suggestions for the configuration assignments for the new bands. The quasiparticle levels relevant in this mass region are given in Table II [10]. The Coriolis interaction mixes the original shell model states in the rotating nucleus. Nevertheless, we include the shell model and Nilsson configurations for convenience.

For the higher-spin states, typically for states with $I > 20$, calculations were performed using the configuration-dependent CNS formalism without pairing [19,35]. The present calculations are similar to those presented for ^{123}Cs in Ref. [21]. Results of these calculations are compared with experimental excitation energies in Figs. 6 and 7 for the positive- and negative-parity bands, respectively.

The CNS configurations are labeled by the number of particles in the different high-j intruder orbitals outside a closed core. However, it should be noted that in this formalism, no separation into core and valence particles is made and all orbitals up to $N = 8$ are treated on an equal footing. In the case of ^{124}Ba, it is natural to choose ^{114}Sn with $Z = 50$ and $N = 64$ as the core. The configurations may then be identified by the number of proton holes in the $g_{9/2}$ subshell, the number of protons in $h_{11/2}$ orbitals, and the number of neutrons in $h_{11/2}$ and $i_{13/2}$ orbitals. The notation for labeling the configurations is given in the form $[(p_0)p_1, n_0(n_1)]$, where p_0 is the number of proton holes in $g_{9/2}$ orbitals (omitted when $p_0 = 0$), p_1 is the number of $h_{11/2}$ protons, n_0 is the number of neutrons in the $h_{11/2}$ subshell, and n_1 the number of neutrons in $i_{13/2}$ orbitals (omitted when $n_1 = 0$). The energy of each configuration is minimized at each spin in the deformation space $(\varepsilon_2, \varepsilon_4, \gamma)$, which allows the development of collectivity to be treated as a function of spin.

TABLE II. Shell model origin and quasiparticle labels for low-lying orbitals in ^{124}Ba.

	Shell model states	Nilsson orbitals	$\alpha = +\frac{1}{2}$	$\alpha = -\frac{1}{2}$
Protons	$(d_{5/2}, g_{7/2})$	$[422]\frac{3}{2}^+$	a	b
	$(d_{5/2}, g_{7/2})$	$[420]\frac{1}{2}^+$	c	d
	$g_{9/2}$	$[404]\frac{9}{2}^+$	a'	b'
	$h_{11/2}$	$[550]\frac{1}{2}^-$	f	e
	$h_{11/2}$	$[541]\frac{3}{2}^-$	h	g
Neutrons	$(s_{1/2}, d_{3/2})$	$[411]\frac{1}{2}^+$	A	B
	$(d_{5/2}, g_{7/2})$	$[402]\frac{5}{2}^+$	C	D
	$(d_{5/2}, g_{7/2})$	$[413]\frac{5}{2}^+$	A'	B'
	$h_{11/2}$	$[523]\frac{7}{2}^-$	F	E
	$h_{11/2}$	$[532]\frac{5}{2}^-$	H	G

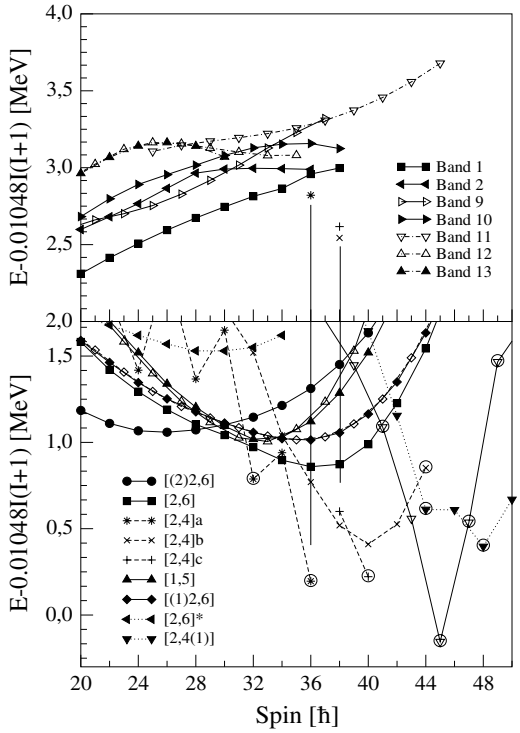

FIG. 6. Experimental excitation energies relative to a rigid-rotor reference as a function of spin for the positive-parity bands in ^{124}Ba (upper panel) compared to energies calculated within the framework of the CNS model (lower panel). Filled and open symbols correspond to signatures $\alpha = 0$ and 1, respectively. For band 11, spins and parity remain uncertain. Vertical lines indicate corresponding experimental and calculated favored noncollective states as discussed in the text.

In the CNS calculations, we used the parameters previously derived for the $A = 130$ region [36]. As pairing is not included, the results should only be compared with experimental data at high spins where pairing is quenched. We note that there is a difference between the absolute values of the experimental and the calculated level energies. The reason is that the experimental level energies are given relative to the ground-state energy, while the reference of the calculated levels is the liquid drop energy at spin zero. Thus, the difference between the experimental and calculated energies depends essentially on the ground-state shell and pairing energy.

The experimental aligned angular momenta and dynamic moments of inertia for bands in ^{124}Ba are shown in Figs. 8 and 9, respectively. The experimental crossing frequencies

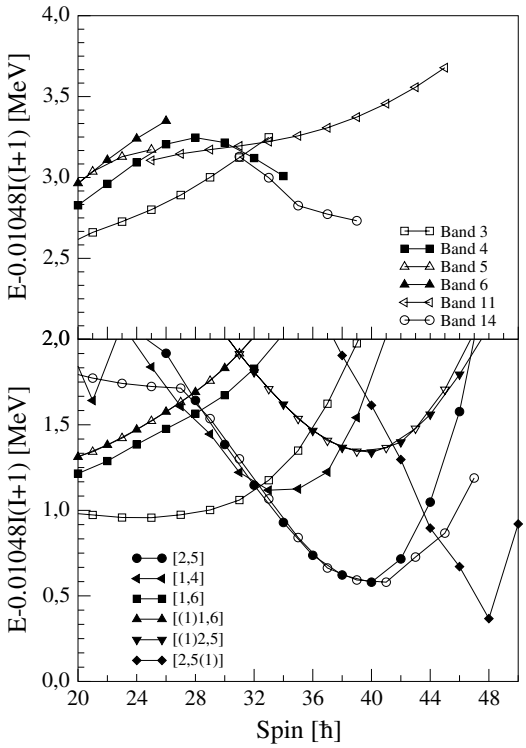

FIG. 7. Experimental excitation energies relative to a rigid-rotor reference as a function of spin for negative-parity bands in ^{124}Ba (upper panel) compared to energies calculated within the framework of the CNS model (lower panel). Filled and open symbols correspond to signatures $\alpha = 0$ and 1, respectively. For bands 11 and 14, spins and parity are not firmly determined.

and the alignment gains are listed in Table III. As can be seen in Fig. 8, up to medium frequencies, the aligned angular momenta i_x increase roughly in two discrete steps, one at low frequencies, around $\hbar\omega = 0.37$ MeV, and another at higher frequencies, around $\hbar\omega = 0.45$ MeV. The alignment gains may be attributed to the decoupling and alignment of quasiparticles of $h_{11/2}$ origin, either $h_{11/2}$ quasiprotons or $h_{11/2}$ quasineutrons. The smaller differences in alignment between the various bands are then caused by different quasiparticles with lower angular momentum j in the configurations. Furthermore, deformation changes and differences in pairing may influence alignments. At the highest observed frequencies, some of the bands show an additional increase in alignment or other irregularities. The band crossings and other irregularities are also visible in the dynamic moments of inertia shown in Fig. 9. In the following, we will discuss the configurations for the various bands.

A. Bands 1 and 2

Band 1 shows band crossings at rotational frequencies of 0.37 and 0.49 MeV/$\hbar$ with alignment gains of 8.2 and 3.3 $\hbar$, respectively, see Fig. 8. The first alignment has been interpreted as crossing of the ground band with the two-quasiproton $h_{11/2}$ band, ef, and the second gain in alignment was suggested to result from a decoupling of an $h_{11/2}$ neutron pair, EF [10]. Therefore, the configuration of band 1 changes from the zero-quasiparticle ground-state band (gsb) to a two-quasiproton configuration, ef, and then to the two-quasiproton-two-quasineutron configuration, $efEF$.

The CNS calculations predict the [2,6] $(\pi h^2_{11/2} \otimes \nu h^6_{11/2})$ configuration to be yrast above spin 28 until it is crossed by the steeply downsloping [2,4] $(\pi h^2_{11/2} \otimes \nu h^4_{11/2})$ configuration, see Fig. 6. At lower spins, the CNS calculations predict the [(2)2,6] $(\pi[(g^{-2}_{9/2})h^2_{11/2}] \otimes \nu h^6_{11/2})$ configuration below the [2,6] structure. However, the calculated relative positions of the [2,6] and [(2)2,6] configurations can depend on the Nilsson parameters, and there is some uncertainty in their relative positions. Indeed, in the neighboring ^{123}Cs nucleus, these calculations also predicted the [(2)2,6] below the [2,6] configuration in that spin region, while the observed alignment frequency favors the [2,6] assignment [21]. The difference may also be due to remnants of pairing at high spins. If pairing is not negligible, [(2)2,6] is a six-quasiparticle configuration while [2,6] is a four-quasiparticle configuration. The extra energy necessary to break a pair in order to form a six-quasiparticle excitation may lift the [(2)2,6] configuration in reality to higher energy than predicted by the CNS calculations which neglect pairing. Thus, band 1 probably corresponds to the [2,6] configuration in the spin region between 22 and 34, in agreement with the previous assignments [10]. The calculated

TABLE III. Experimental crossing frequencies and aligned angular momenta in ^{124}Ba.

Band	Config. before crossing	i_x [$\hbar$]	$\hbar\omega_c$ [MeV]	Δi_x [$\hbar$]	Config. above 1st crossing	$\hbar\omega_c$ [MeV]	Δi_x [$\hbar$]	Config. above 2nd crossing	$\hbar\omega_c$ [MeV]	Δi_x [$\hbar$]
1	0-qp	0	0.37	8.2	*ef*	0.49	3.3	*efEF*	–	–
2	0-qp	0	0.41	6.2	*EF*	0.44	4.4	*EF ef*	0.63	2.5
3	*eb*	$\approx$ 5.1	0.46	6.0	*eb EF*	–	–	–	–	–
4	*ea*	5.4	0.44	4.0	*ea GH*	0.59	$\approx$6.0	*eaGHEF*	–	–
5	*eb′*	5.8	0.44	> 6.1	*eb′ EF*	–	–	–	–	–
6	*ea′*	5.8	0.44	> 5.8	*ea′ EF*	–	–	–	–	–
9	*efGH*	11	–	–	–	–	–	–	–	–
10	*efFH*	9.5	–	–		–	–	–	–	–
12	*eb′ EA′*	8.5	0.52	5.2	*eb′ EA′GH*	–	–	–	–	–
13	*eb′ FA′*	8.5	0.52	4.9	*eb′ FA′GH*	0.64	>2.5	–	–	–

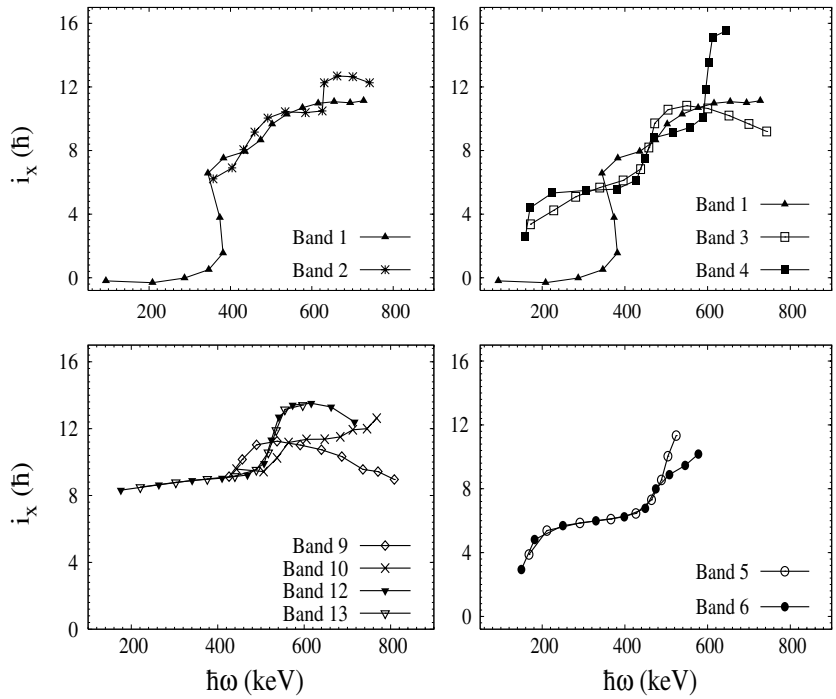

FIG. 8. Aligned angular momentum i_x as a function of rotational frequency. A reference core with Harris parameters $\mathcal{J}_\circ = 17\,\hbar^2\,\mathrm{MeV}^{-1}$ and $\mathcal{J}_1 = 26\,\hbar^4\,\mathrm{MeV}^{-3}$ has been subtracted [37].

shape parameters for this configuration are $\varepsilon_2 \approx 0.24$ and $\gamma \approx 0^\circ$.

Above the $I^\pi = 34^+$ state, band 1 becomes irregular and forks into three branches, see Fig. 1. This is the typical behavior expected for band termination. Terminating bands were first observed in the Dy-Er region [38]. However, there exist analogies between the $A = 160$ and 125 mass regions [20]. As illustrated in Fig. 10, four protons in $h_{11/2}$ orbitals outside the $Z = 64$ semiclosed core in ^{156}Er may be compared to four neutrons in $h_{11/2}$ orbitals in ^{124}Ba, which has $N = 68$ neutrons. Similarly, six neutrons above the $N = 82$ closed core in ^{156}Er is analogous to six protons outside the $Z = 50$ closed core in ^{124}Ba. Thus, the observed fully aligned configuration $\pi(h_{11/2})^4_{16} \otimes \nu[(h_{9/2})^2_8(f_{7/2})^2_6(i_{13/2})^2_{12}]$ of the $I^\pi = 42^+$ state in ^{156}Er [39] is analogous to the configuration $\pi[(h_{11/2})^2_{10}(g_{7/2}d_{5/2})^4_{10}] \otimes \nu(h_{11/2})^4_{16}$ with $I^\pi = 36^+$ in ^{124}Ba.

The present CNS calculations agree well with the expectations based on this analogy. In Fig. 6, we differentiated between three types of states of the [2,4] configuration defined above. The configuration [2,4]a denotes the states with only

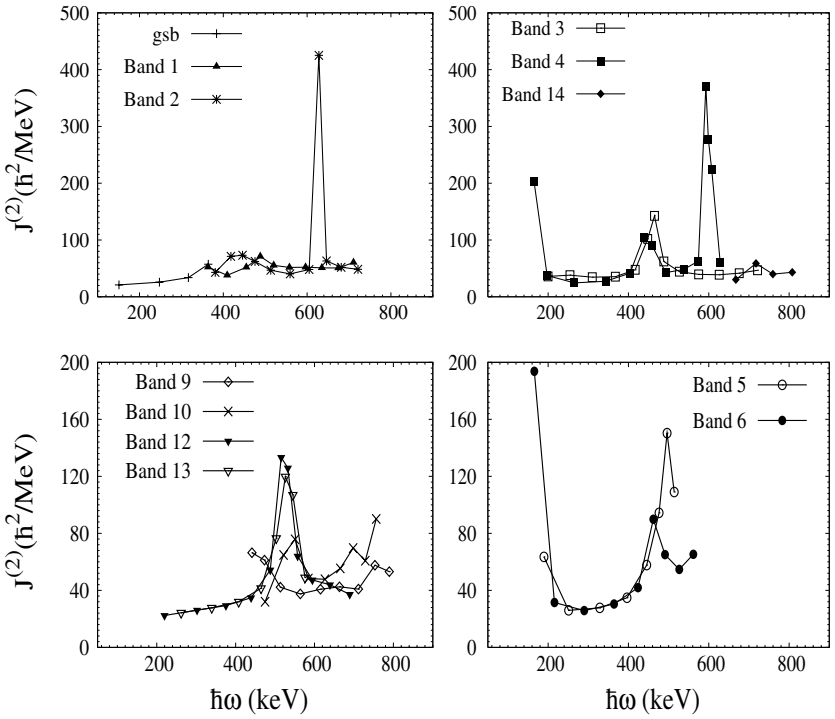

FIG. 9. Dynamic moment of inertia $\mathcal{J}^{(2)}$ as a function of rotational frequency taken as $\hbar\omega = E_\gamma/2$ for all observed bands.

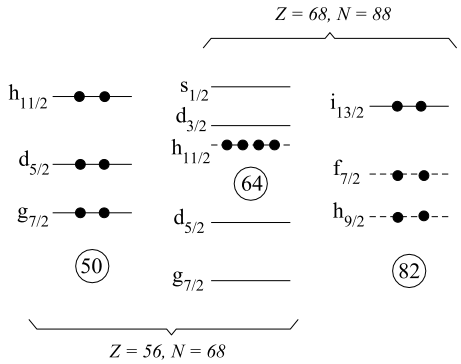

FIG. 10. Analogy between $A = 125$ and 160 mass regions: filling of subshells outside the ^{114}Sn and ^{146}Gd cores is illustrated schematically.

four valence neutrons relative to the $N = 64$ core, and they all are located in the $h_{11/2}$ subshell, while [2,4]b and [2,4]c correspond to the states where one neutron and two neutrons, respectively, are excited from the $d_{5/2}g_{7/2}$ subshell to the $s_{1/2}d_{3/2}$ orbitals. The [2,4]a configuration is predicted to become yrast around spin 34 and to terminate at $I^\pi = 36^+$ in a strongly favored state. Two favored 38^+ states and two favored 40^+ states are predicted corresponding to the [2,4]b and [2,4]c configurations. Experimentally, we observe two 36^+ states and three 38^+ states. Comparing the relative positions of the calculated states with different configurations with the relative positions of the observed bands shown in Fig. 6, it is most likely that the [2,4]a $(\pi[(h_{11/2})^2_{10}(g_{7/2}d_{5/2})^4_{10}] \otimes \nu(h_{11/2})^4_{16})$ terminating configuration has to be assigned to the yrast 36^+ state. This is a noncollective oblate state, characterized by the deformation parameters $\varepsilon_2 \approx 0.2$ and $\gamma = 60^\circ$. Its total angular momentum is built solely from the maximally aligned angular momenta of the valence particles corresponding to the [2,4]a configuration. Comparing the relative positions of the two higher-energy nearly degenerate 36^+ states, they probably correspond to the [2,6] and [2,4]b configurations, respectively. Similarly, the two lowest strongly favored 38^+ states probably correspond to the [2,4]b and [2,4]c configurations, respectively, while the highest-energy 38^+ state has the [2,6] configuration. The 38^+ states belonging to [2,4]b and [2,4]c are partially aligned, and these configurations are expected to terminate at spins 44 and 40, respectively. We note here that the predicted [2,4] structure in ^{124}Ba is very similar to the predicted [1,4] structure in ^{123}Cs [21], but with an additional $h_{11/2}$ proton. Therefore, the 36^+ state is analogous to the $63/2^-$ terminating state in ^{123}Cs. As shown in Ref. [21], the states around this spin in ^{123}Cs are due to energy minima in the potential energy surface corresponding to zero, one, and two particle-hole excitations from neutron $(d_{5/2}g_{7/2})$ to $(s_{1/2}d_{3/2})$ orbitals. Calculations for ^{124}Ba also show the existence of these minima around spin 36.

Band 2 starts with an alignment of about 6.2 $\hbar$ (see Fig. 8) and shows a band crossing with an alignment gain of 4.4 $\hbar$ at a frequency of 0.44 MeV/$\hbar$. Previously, the two-quasineutron configuration EF, of $\nu h_{11/2}$ origin, was assigned to this band below 0.44 MeV/$\hbar$. At this frequency, the decoupling of an $h_{11/2}$ quasiproton pair takes place and the configuration changes to the two-quasineutron-two-quasiproton $(\nu h^2_{11/2} \otimes \pi h^2_{11/2})$ structure, $EFef$ [10]. In this frequency range, band 1 has the same configuration. However, in band 2, the $h_{11/2}$ quasineutron pair is almost fully aligned ($\approx$6.2 $\hbar$) and the $h_{11/2}$ quasiproton pair is only partially aligned (4.4 $\hbar$), whereas in band 1 it is opposite: the $h_{11/2}$ quasiproton pair is nearly fully aligned (8.2 $\hbar$) and the $h_{11/2}$ quasineutron pair shows a smaller alignment (3.3 $\hbar$). The close similarity of the configurations of bands 1 and 2 results in the strong decay from the higher-lying band 2 into the yrast band 1.

In the calculations using the CNS formalism, the configurations above the first two band crossings in bands 1 and 2 are the same; i.e., both are represented by a pair of aligned $h_{11/2}$ protons and $h_{11/2}$ neutrons, although with a different distribution of the valence protons and neutrons in low-j orbitals. Indeed, a second minimum appears in the calculations with shape parameters $\varepsilon_2 \approx 0.24$ and $\gamma \approx -30^\circ$. The corresponding configuration is labeled [2,6]* in Fig. 6. This minimum becomes more and more shallow with increasing spin and disappears above spin 34. However, the calculated relative energy difference between the first and second minimum does not agree well with that observed for bands 1 and 2. At spin 22, both the calculated and experimental energy differences are $\approx$250 keV. This difference is predicted to increase with increasing spin up to $\approx$700 keV, while experimentally it is constant up to $I = 28$ and continuously decreases above this spin to about 30 keV. This behavior indicates a change in the configuration around spin 28. According to Fig. 6, a possible candidate for the configuration above this spin can be [2,4]b which is predicted to cross the [2,6] configuration at spin 36.

The alignment of band 2 (Fig. 8) shows an irregularity at $\hbar\omega = 0.63$ MeV with an alignment gain of 2.5 $\hbar$, which is not seen in band 1. In the yrast bands of the neighboring even-even nuclei ^{126}Ba [11] and ^{128}Ba [13], a similar behavior with alignment gains of $\approx$2 and $\approx$4 $\hbar$, respectively, has been observed. The alignment of a pair of protons of $g_{7/2}$ origin was suggested for the crossing around $\hbar\omega = 0.6$ MeV in ^{126}Ba [11], whereas an alignment of a second pair of $h_{11/2}$ neutrons was proposed for the crossing at this frequency in ^{128}Ba [13]. These may be alternative explanations for the behavior of band 2 at high spins in ^{124}Ba.

B. Coupled bands

Information about the quasiparticle configurations of the coupled bands can be extracted from the ratios of reduced magnetic dipole and electric quadrupole transition probabilities, $B(M1; I \to I-1)/B(E2; I \to I-2)$. The experimental ratios have been obtained from the γ-ray-intensity ratios using

$$\frac{B(M1; I \to I-1)}{B(E2; I \to I-2)} = 0.697 \frac{I_\gamma(M1; I \to I-1)}{I_\gamma(E2; I \to I-2)} \times \frac{E^5_\gamma(E2)}{E^3_\gamma(M1)} \frac{1}{1+\delta^2} \left(\frac{\mu_N}{e\,\mathrm{b}}\right)^2,$$

where E_γ and I_γ represent the energy in MeV and the intensity of the γ-ray transitions, respectively. The mixing ratio δ for the $\Delta I = 1$ transitions is small, and δ^2 has been set to zero. The experimentally deduced $B(M1)/B(E2)$ ratios are compared with the theoretical values obtained using the following generalized expression for multiquasiparticle configurations, formulated in [2,40] and based on the geometrical model of Dönau and Frauendorf [41,42]:

$$\frac{B(M1; I \to I-1)}{B(E2; I \to I-2)} = \frac{12}{5Q_\circ^2 \cos^2(\gamma + 30^\circ)} \left[1 - \frac{K_{\rm tot}^2}{\left(I - \frac{1}{2}\right)^2}\right]^{-2} \left\{\left(I - \frac{K_{\rm tot}^2}{I^2}\right)^{1/2} \times \left[K_1(g_1 - g_R)\left(1 \pm \frac{\Delta e'}{\hbar\omega}\right) + \sum_\lambda K_\lambda (g_\lambda - g_R)\right] - \frac{K_{\rm tot}}{I}\left[(g_1 - g_R) i_1 + \sum_\lambda (g_\lambda - g_R) i_\lambda\right]\right\}^2 .$$

K_λ, g_λ, and i_λ stand for the K value, gyromagnetic factor, and aligned angular momentum, respectively, of the rotation- or Fermi-aligned quasiparticles involved in the configuration. K_1, g_1, and i_1 refer to the strongly coupled particle. The approximation $g_R = Z/A$ was used for the rotational g factor. $K_{\rm tot} = K_1 + \sum_\lambda K_\lambda$ denotes the total K value of the configuration. The values for the intrinsic g factors for the different orbitals g_λ, as well as the quadrupole moment $Q_\circ = 3.9$ b, have been taken from [11]. The shape parameter γ was set to zero. The aligned angular momenta i_m were determined from the alignment plots, see Fig. 8. The signature splitting $\Delta e'$ was extracted from the experimental Routhians. The parameters used in the calculations are listed in Table IV.

TABLE IV. Gyromagnetic factors and alignments used for the calculation of $B(M1)/B(E2)$ ratios.

Bands	Subshell	Nilsson orbital	g factor	K	$i[\hbar]$
3,4	$\pi h_{11/2}$	$[550]\frac{1}{2}^-$	1.17	0.5	5.0
	$\pi g_{7/2}$	$[422]\frac{3}{2}^+$	0.72	1.5	1.0
	$\pi d_{5/2}$	$[420]\frac{1}{2}^+$	1.38	0.5	1.0
5,6	$\pi h_{11/2}$	$[550]\frac{1}{2}^-$	1.17	0.5	5.0
	$\pi g_{9/2}$	$[404]\frac{9}{2}^+$	1.27	4.5	1.0
12,13	$\pi h_{11/2}$	$[550]\frac{1}{2}^-$	1.17	0.5	5.0
	$\pi d_{5/2}$	$[420]\frac{1}{2}^+$	1.38	0.5	1.0
	$\pi g_{9/2}$	$[404]\frac{9}{2}^+$	1.27	4.5	0.0
	$\nu h_{11/2}$	$[532]\frac{5}{2}^-$	−0.21	2.5	3.5
		$[541]\frac{3}{2}^-$	−0.21	1.5	3.5
	$\nu g_{7/2}$	$[402]\frac{5}{2}^+$	0.21	–	0.5
		$[404]\frac{7}{2}^+$	0.21	3.5	0.5
	$\nu d_{5/2}$	$[413]\frac{5}{2}^+$	−0.33	2.5	0.5

1. Bands 3, 4, and 14

Bands 3 and 4 appear to be a pair of signature-partner bands with a large splitting. It was suggested [10] that band 3 (the favored signature) corresponds to the quasiproton $e\,b$ configuration, and band 4 (the unfavored signature) to ea or ec. The $\pi h_{11/2} g_{7/2}$ and $\pi(h_{11/2} d_{5/2}) \otimes \nu h_{11/2}^4$ configurations were also assigned to similar bands in the neighboring even-even nuclei ^{126}Ba [11] and ^{128}Ba [13], respectively. It was suggested [30,32,43] that those bands have a two-quasiproton structure mixed with the octupole vibrational band which accounts for the large signature splitting at low spins. Both bands are crossed by the configuration with an additional $h_{11/2}$ quasineutron pair, EF.

The $B(M1)/B(E2)$ ratios determined from our data for bands 3 and 4 are compared with the calculated values for the configurations $\pi h_{11/2} g_{7/2}$ and $\pi h_{11/2} d_{5/2}$ in Fig. 11. The calculated ratios for the configuration $\pi h_{11/2} d_{5/2}$ agree better with the experimental data than those for the $\pi h_{11/2} g_{7/2}$ configuration. Therefore, we assign the configuration $\pi h_{11/2} d_{5/2}$ to bands 3 and 4 in the low-spin region. At higher spins, these configurations are expected to become more and more mixed.

Both bands show a band crossing at a rotational frequency of ≈0.45 MeV/$\hbar$ with a gain in alignment of 6 and 4 $\hbar$, respectively. The rather large alignment suggests that aligned $h_{11/2}$ neutrons or protons are present in the configuration above that frequency. We suggest the configurations $ebEF$ and $eaGH$ for bands 3 and 4, respectively, in the frequency range around 0.5 MeV/$\hbar$. At higher frequencies, band 3 seems to lose alignment, see Fig. 8. However, this might be caused by a change to a reference core with a smaller deformation. A reduction of the Harris parameters to $\mathcal{J}_\circ = 13\,\hbar^2$ MeV^{-1} and $\mathcal{J}_1 = 21\,\hbar^4$ MeV^{-3} makes the alignment of band 3 constant.

Band 4 shows a gain in alignment of ≈6 $\hbar$ at a frequency of 0.59 MeV/$\hbar$ (Fig. 8). Such a large gain can only be caused by

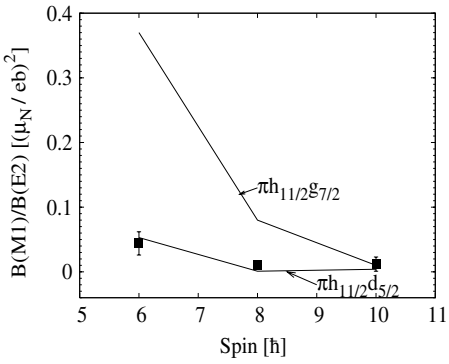

FIG. 11. $B(M1)/B(E2)$ ratios derived from measured γ-ray branching ratios for bands 3 and 4 and calculated values for the $\pi h_{11/2} d_{5/2}$ and $\pi h_{11/2} g_{7/2}$ configurations.

$h_{11/2}$ neutrons or protons. As band 3 does not show a similar increase at that frequency, the corresponding alignment has to be blocked. Thus, it is most likely that it is caused by a pair of $h_{11/2}$ neutrons, e.g., *EF*, which are already aligned in band 3 at this frequency. At the highest observed frequencies, the configuration *eaGHEF* is therefore suggested for band 4.

At high spins, the [1,6] configuration is suggested by the CNS calculations. As seen in Fig. 7, there is good agreement for the relative positions and slopes between the calculated [1,6] bands and the observed bands 3 and 4 up to spin 26.

Band 14 decays into band 3 around spin 30. Unfortunately, its spin assignment is not certain. If our tentative assignment is correct, band 14 has an alignment that is $\approx 5\,\hbar$ higher than that of band 3, which could be explained by a six-quasiparticle configuration.

2. Bands 5 and 6

Bands 5 and 6 form a pair of signature partners with negligible signature splitting. The two-quasiproton configurations eb' and ea', of $g_{9/2}h_{11/2}$ origin, seem to be a natural choice for these bands [10]. At a frequency of 0.44 MeV/$\hbar$, a band crossing with an alignment gain of >6.1 and $>5.8\,\hbar$ is observed for bands 5 and 6, respectively. The high-spin part of the bands probably contains a pair of decoupled $h_{11/2}$ neutrons, resulting in the configurations $eb'EF$ and $ea'EF$, respectively.

$B(M1)/B(E2)$ ratios have been determined and are compared with calculated ratios for the $\pi g_{9/2}h_{11/2}$ configuration in Fig. 12. At lower spins, a rather large $B(M1)/B(E2)$ ratio has been obtained. In this region, mixing occurs with other states of the same spin and parity which also accounts for the observed decay-out transitions. Large $B(M1)/B(E2)$ ratios are calculated for configurations involving neutrons, e.g., for the $\nu h_{11/2}g_{7/2}$ or $\nu h_{11/2}s_{1/2}$ configurations. Mixing with such states may explain the observed increase of the $B(M1)/B(E2)$ ratios near the bottom of bands 5 and 6. The good agreement at medium spins supports the previous configuration assignment [10] which corresponds to the [(1)1,6] CNS configuration. The theoretically predicted relative positions and slopes of this configuration are in agreement with those of bands 5 and 6, as seen in Fig. 7.

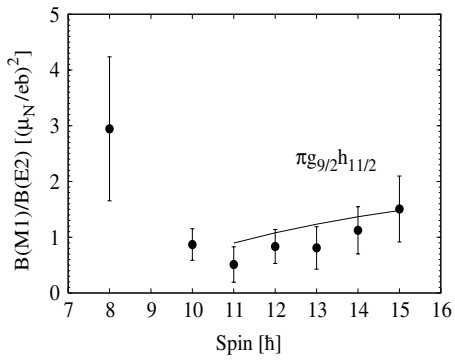

FIG. 12. $B(M1)/B(E2)$ ratios derived from measured γ-ray branching ratios for bands 5 and 6 and calculation for the $\pi g_{9/2}h_{11/2}$ configuration.

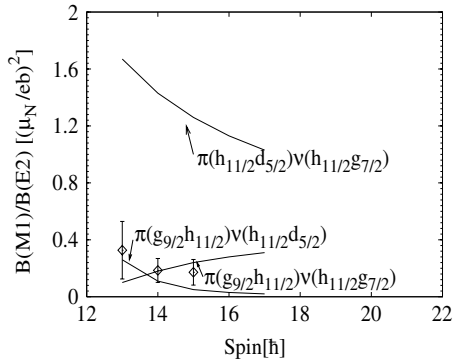

FIG. 13. $B(M1)/B(E2)$ ratios derived from measured γ-ray branching ratios for bands 12 and 13 and calculated ratios for three different configurations.

3. Bands 7 and 8

Bands 7 and 8 have been interpreted previously to be built on a γ vibration [16,44]. The present results do not add significant information about these bands.

4. Bands 12 and 13

The new bands 12 and 13 form a pair of coupled bands without signature splitting. Their alignment is already rather large, $i_x \geqslant 8\,\hbar$, at low rotational frequencies, suggesting a multiquasiparticle configuration. The experimental $B(M1)/B(E2)$ ratios determined from our data are compared with calculations for three different configurations, $\pi(h_{11/2}d_{5/2}) \otimes \nu(h_{11/2}g_{7/2})$, $\pi(g_{9/2}h_{11/2}) \otimes \nu(h_{11/2}g_{7/2})$, and $\pi(g_{9/2}h_{11/2}) \otimes \nu(h_{11/2}d_{5/2})$, in Fig. 13. As can be seen, the calculated ratios for the configurations $\pi(g_{9/2}h_{11/2}) \otimes \nu(h_{11/2}g_{7/2})$ and $\pi(g_{9/2}h_{11/2}) \otimes \nu(h_{11/2}d_{5/2})$ are close to the experimental data. These configurations are expected to be mixed, and it is not possible to distinguish between them. Thus, we assign the configurations $eb'EA'$ and $eb'FA'$ to bands 12 and 13, respectively.

At a frequency of $\omega = 0.5$ MeV/$\hbar$, a further band crossing is observed. The alignment gain of about $5\,\hbar$ may be due to a pair of $h_{11/2}$ neutrons. As orbitals *E* and *F* are already occupied, we suggest that the alignment is due to the *GH* quasineutron pair.

Two band structures with small signature splitting, the [1,5] and [(1)2,6] configurations, are predicted by the present CNS calculations. They approach the yrast [2,6] configuration in the spin 20–35 region, see Fig. 6. The experimental energy difference between the [1,5] and [2,6] configurations is predicted to decrease up to about spin 32 and then to increase at higher spins. For the [(1)2,6] configuration, this energy difference is predicted to increase continuously in that spin region. The energy difference between band 1 and bands 12 and 13 decreases above spin 24 and becomes very small in the spin 30–35 region. This observation favors the [1,5] assignment over the [(1)2,6] configuration. Another argument against the [(1)2,6] configuration is that, similar to the case of the [(2)2,6] configuration discussed above, it may in reality lie at a higher

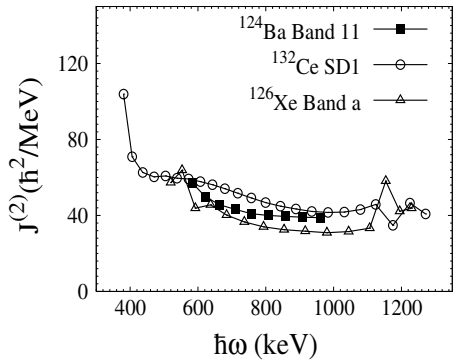

FIG. 14. Dynamic moment of inertia $\mathcal{J}^{(2)}$ for band 11 in ^{124}Ba as well as for similar bands in ^{132}Ce [45] and ^{126}Xe [46], as a function of rotational frequency.

energy than predicted because of the pairing interaction which is not taken into account in the CNS calculations.

C. Bands 9 and 10

The new bands 9 and 10 are observed above spins 17 and 18, respectively. They both decay into band 1, suggesting a similarity in structure. They start with a high alignment which, in the lower part, increases by about 3 $\hbar$ and then stays at 11 and 9.5 $\hbar$, respectively (Fig. 8). At higher spins, their alignment pattern looks different. While the alignment of band 9 decreases, band 10 continuously gains alignment up to the highest-spin states observed. The rather large alignment suggests that both bands are four-quasiparticle configurations, probably containing a pair of aligned protons coupled to another aligned proton or a neutron pair. We tentatively assign the quasiparticle configurations *efGH* and *efFH* to bands 9 and 10, respectively. The difference in the appearance of the alignment might be caused by differences in the reference core. A reduction of the Harris parameters for band 9 to $\mathcal{J}_\circ = 13\ \hbar^2\ \mathrm{MeV}^{-1}$ and $\mathcal{J}_1 = 21\ \hbar^4\ \mathrm{MeV}^{-3}$ makes its alignment constant.

Inspection of the results of the CNS calculations presented in Fig. 6 shows that the configuration labeled [1,5] could reproduce the observed properties reasonably well. However, it seems unlikely that bands 9 and 10 are a pair of signature partners since no interband transitions are observed. Furthermore, we have already tentatively assigned this configuration to bands 12 and 13, as discussed above. Thus, there are no good candidates predicted by the present CNS calculations for the configurations of these bands.

D. Band 11

Band 11 is not firmly connected to known levels in ^{124}Ba. However, the systematics of excitation energies and spins of the bands observed in this nucleus allow an approximate placement in the level scheme and limit the spin range. As the band decays to high-spin states of band 1, their structures should have some similarity.

Band 11 is observed only above spin 25 or 26 and continues without band crossing up to spin 45 or 46. The most likely candidate from the CNS calculations is the [2,5(1)] configuration, i.e., $\pi h_{11/2}^2 \otimes \nu h_{11/2}^5 i_{13/2}$. In its decay to band 1, it goes over to the [2, 6] configuration with two $h_{11/2}$ protons and six $h_{11/2}$ neutrons.

Band 11 shows a gradual decrease in the dynamic moment of inertia in a manner similar to that of several high-spin bands in this mass region. In Fig. 14, the dynamic moments of inertia of band 11 and similar bands observed in ^{132}Ce [45,47,48] and ^{126}Xe [46] are compared. The ^{132}Ce band is highly deformed; a transition quadrupole moment of Q = 7.4 (3) b has been measured [47]. In ^{125,126}Xe, several bands, which extend up to very high spins, have been observed recently [46]. However, only for the ^{126}Xe band shown in Fig. 14 was the quadrupole moment estimated, $Q \sim 5.2$ b [46]. The dynamic moment of inertia of band 11 lies between those of ^{126}Xe and ^{132}Ce shown in Fig. 14. This systematics suggests that it probably has a larger deformation than the other bands in ^{124}Ba. The excitation of an $i_{13/2}$ neutron may cause the larger deformation; however, lifetime measurements are needed for a final proof. CSM calculations for ^{132}Ce show that the frequency dependence of the dynamic moment of inertia is a combined effect of gradual alignment of protons in $h_{11/2}$ and neutrons in $h_{9/2}$ and $h_{11/2}$ orbitals [49]; a similar explanation may apply also to band 11 in ^{124}Ba.

V. SUMMARY

In summary, high-spin states in ^{124}Ba have been investigated in two experiments using the Euroball and Gammasphere spectrometers. Previously known bands have been extended, and six new bands have been found. Configurations have been assigned to the band structures based on the comparison with predictions of the CSM in the lower-spin region and with the CNS model at high spins. The positive-parity yrast band, band 1, shows the typical behavior of band termination at the highest spins. Configurations for the terminating states which compete with the collective excitations are suggested on the basis of CNS calculations. One of the new bands, band 11, extends to spins around 46 without band crossings. Its dynamic moment of inertia decreases steadily, similar to those of large-deformed bands in this mass region.

ACKNOWLEDGMENTS

The authors are grateful to I. Ragnarsson for helpful discussions of the results of the CSN calculations and the configuration assignments to the band structures in ^{124}Ba. This work was supported in part by the EU (Contract No. EUROVIV: HPRI-CT-1999-00078), the German BMBF (Contract Nos. 06 BN 907), the Hungarian Scientific Research Fund OTKA (Contract Nos. T046901 and T038404), the Bolyai János Foundation of HAS, and by INFN, Italy, and the Polish Ministry of Education and Science (Grant No. 1 P03B 030 30).

[1] F. Seiffert, W. Lieberz, A. Dewald, S. Freund, A. Gelberg, A. Granderath, D. Lieberz, R. Wirowski, and P. von Brentano, Nucl. Phys. **A554**, 287 (1993).

[2] S. Törmänen, S. Juutinen, R. Julin, B. Cederwall, A. Johnson, R. Wyss, P. Ahonen, B. Fant, M. Matsuzaki, J. Nyberg *et al.*, Nucl. Phys. **A572**, 417 (1994).

[3] H. Timmers, J. Simpson, M. A. Riley, T. Bengtsson, M. A. Bentley, F. Hanna, S. M. Mullins, J. F. Sharpey-Schafer, and R. Wyss, J. Phys. G: Nucl. Part. Phys. **A20**, 287 (1994).

[4] J. Timár, J. Simpson, E. S. Paul, S. Araddad, C. W. Beausang, M. A. Bentley, M. J. Joyce, and J. F. Sharpey-Schafer, J. Phys. G: Nucl. Part. Phys. **21**, 783 (1995).

[5] I. Wiedenhöver, J. Yan, U. Neuneyer, R. Wirowski, P. von Brentano, A. Gelberg, N. Yoshida, and T. Otsuka, Nucl. Phys. **A582**, 77 (1995).

[6] M. Serris, C. T. Papadopoulos, R. Vlastou, C. A. Kalfas, S. Kossionides, N. Fotiades, S. Harissopulos, C. W. Beausang, M. J. Joyce, E. S. Paul *et al.*, Z. Phys. A **358**, 37 (1997).

[7] I. Schneider, R. S. Chakrawarthy, I. Wiedenhöver, A. Schmidt, H. Meise, P. Petkov, A. Dewald, P. von Brentano, O. Stuch, K. Jessen *et al.*, Phys. Rev. C **60**, 014312 (1999).

[8] V. Werner, H. Meise, I. Wiedenhöver, A. Gade, and P. von Brentano, Nucl. Phys. **A692**, 451 (2001).

[9] R. Wyss, A. Granderath, R. Bengtsson, P. von Brentano, A. Dewald, A. Gelberg, A. Gizon, J. Gizon, S. Harissopulos, A. Johnson *et al.*, Nucl. Phys. **A505**, 337 (1989).

[10] S. Pilotte, S. Flibotte, S. Monaro, N. Nadon, N. Prevost, P. Taras, H. R. Andrews, D. Horn, V. P. Janzen, D. C. Radford *et al.*, Nucl. Phys. **A514**, 545 (1990).

[11] D. Ward, V. P. Janzen, H. R. Andrews, D. C. Radford, G. C. Ball, D. Horn, J. C. Waddington, J. K. Johansson, F. Banville, J. Gascon *et al.*, Nucl. Phys. **A529**, 315 (1991).

[12] A. Granderath, P. F. Mantica, R. Bengtsson, R. Wyss, P. von Brentano, A. Gelberg, and F. Seiffert, Nucl. Phys. **A597**, 427 (1996).

[13] O. Vogel, R. S. Chakrawarthy, A. Dewald, P. Petkov, K. Jessen, J. Gableske, P. von Brentano, D. Bazzacco, A. Gizon, J. Gizon *et al.*, Eur. Phys. J. A **4**, 323 (1999).

[14] C. M. Petrache, G. LoBianco, D. Bazzacco, T. Kröll, S. Lunardi, R. Menegazzo, M. Nespolo, P. Pavan, C. R. Alvarez, G. de Angelis *et al.*, Eur. Phys. J. A **12**, 135 (2001).

[15] J. F. Smith, C. J. Chiara, D. B. Fossan, G. J. Lane, J. M. Sears, I. Thorslund, I. M. Hibbert, R. Wadsworth, I. Y. Lee, and A. O. Macchiavelli, Phys. Lett. **B483**, 7 (2000).

[16] J. P. Martin, V. Barci, H. El-Samman, A. Gizon, J. Gizon, W. Klamra, B. M. Nyakó, F. A. Beck, T. Byrski, and J. C. Merdinger, Nucl. Phys. **A489**, 169 (1988).

[17] C. M. Petrache, G. LoBianco, P. G. Bizzeti, A. M. Bizzeti-Sona, D. Bazzacco, S. Lunardi, M. Nespolo, G. de Angelis, D. R. Napoli, N. Blasi *et al.*, Eur. Phys. J. A **16**, 337 (2003).

[18] J. F. Smith, V. Medina-Chico, C. J. Chiara, M. P. Carpenter, C. N. Davids, M. Devlin, J. L. Durell, D. B. Fossan, S. J. Freeman, R. V. F. Janssens *et al.*, Phys. Rev. C **69**, 034339 (2004).

[19] A. V. Afanasjev, D. B. Fossan, G. J. Lane, and I. Ragnarsson, Phys. Rep. **322**, 1 (1999).

[20] I. Ragnarsson, Z. Xing, T. Bengtsson, and M. A. Riley, Phys. Scr. **34**, 651 (1986).

[21] A. K. Singh, H. Hübel, J. Domscheit, G. B. Hagemann, B. Herskind, D. R. Jensen, J. N. Wilson, R. Clark, M. Cromaz, P. Fallon *et al.*, Phys. Rev. C **70**, 034315 (2004).

[22] A. Al-Khatib, A. K. Singh, H. Hübel, P. Bringel, A. Bürger, A. Neußer-Neffgen, G. Schönwaßer, G. Hagemann, C. R. Hansen, B. Herskind *et al.*, Acta Phys. Pol. B **36**, 1029 (2005).

[23] H. Hübel, Acta Phys. Pol. B **36**, 1015 (2005).

[24] I. Y. Lee, Nucl. Phys. **A520**, 641c (1990).

[25] F. A. Beck, Prog. Part. Nucl. Phys. **28**, 443 (1992).

[26] J. Simpson, Z. Phys. A **358**, 139 (1997).

[27] J. N. Scheurer, M. Aiche, M. M. Aleonard, G. Barreau, F. Bourgine, D. Boivin, D. Cabaussel, J. F. Chemin, T. P. Doan, J. P. Goudour *et al.*, Nucl. Instrum. Methods A **385**, 501 (1997).

[28] J. Gál, G. Hegyesi, J. Molnár, B. M. Nyakó, G. Kalinka, J. N. Scheurer, M. M. Aléonard, J. F. Chemin, J. L. Pedroza, K. Juhász *et al.*, Nucl. Instrum. Methods A **516**, 502 (2004).

[29] D. C. Radford, Nucl. Instrum. Methods A **361**, 297 (1995).

[30] P. Mason, G. Benzoni, A. Bracco, F. Camera, B. Million, O. Wieland, S. Leoni, A. K. Singh, A. Al-Khatib, H. Hübel *et al.*, Phys. Rev. C **72**, 064315 (2005).

[31] D. Roßbach, A. Görgen, H. Hübel, E. Mergel, G. Schönwaßer, A. N. Wilson, F. Azaiez, A. Astier, D. Bazzacco, M. Bergström *et al.*, Phys. Lett. **B513**, 9 (2001).

[32] R. Piepenbring and J. Leandri, Phys. Lett. **B267**, 17 (1991).

[33] R. Bengtsson and S. Frauendorf, Nucl. Phys. **A314**, 27 (1979).

[34] R. Bengtsson, S. Frauendor, and F. R. May, At. Data Nucl. Data Tables **35**, 15 (1986).

[35] T. Bengtsson and I. Ragnarsson, Nucl. Phys. **A436**, 14 (1985).

[36] D. M. Todd, R. Aryaeinejad, D. J. G. Love, A. H. Nelson, P. J. Nolan, P. J. Smith, and P. J. Twin, J. Phys. G: Nucl. Part. Phys. **10**, 1407 (1984).

[37] A. V. Afanasjev and I. Ragnarsson, Nucl. Phys. **A608**, 176 (1996).

[38] A. V. Afanasjev and I. Ragnarsson, Nucl. Phys. **A591**, 387 (1995).

[39] F. S. Stephens, M. A. Deleplanque, R. M. Diamond, A. O. Macchiavelli, and J. E. Draper, Phys. Rev. Lett. **54**, 2584 (1985).

[40] D. C. Radford, H. R. Andrews, G. C. Ball, D. Horn, D. Ward, F. Banville, S. Flibotte, S. Monaro, S. Pilotte, P. Taras *et al.*, Nucl. Phys. **A545**, 665 (1992).

[41] F. Dönau and S. Frauendorf, in *Proceedings of the Conference on High Angular Momentum Properties of Nuclei (Oak Ridge, 1982)*, edited by N. R. Johnson (Harwood Academic, New York, 1983), p. 143.

[42] F. Dönau, Nucl. Phys. **A471**, 469 (1987).

[43] R. Wyss, A. Johnson, D. J. G. Love, M. J. Godfrey, and S. M. Mullins, Z. Phys. A **332**, 241 (1989).

[44] T. Komatsubara, T. Hosoda, H. Sakamoto, T. Aoki, and K. Furuno, Nucl. Phys. **A496**, 605 (1989).

[45] E. S. Paul, P. T. W. Choy, C. Andreoiu, A. J. Boston, A. O. Evans, C. Fox, S. Gros, P. J. Nolan, G. Rainovski, J. A. Sampson *et al.*, Phys. Rev. C **71**, 054309 (2005).

[46] C. R. Hansen, G. B. Hagemann, B. Herskind, D. R. Jensen, G. Sletten, J. N. Wilson, S. O. Degård, P. Bringel, C. Engelhardt, H. Hübel *et al.*, AIP Conf. Proc. **764**, 46 (2005).

[47] R. M. Clark, I. Y. Lee, P. Fallon, D. T. Joss, S. J. Asztalos, J. A. Becker, L. Bernstein, B. Cederwall, M. A. Deleplanque, R. M. Diamond, L. P. Farris, K. Hauschild, W. H. Kelly, A. O. Macchiavelli, P. J. Nolan, and N. O'Brien, Phys. Rev. Lett. **76**, 3510 (1996).

[48] P. J. Nolan, A. Kirwan, D. J. G. Love, A. H. Nelson, D. J. Unwin, and P. J. Twin., J. Phys. G: Nucl. Part. Phys. **11**, L17 (1985).

[49] R. Wyss, J. Nyberg, A. Johnson, R. Bengtsson, and W. Nazarewicz, Phys. Lett. **B215**, 211 (1988).